Guided Tissue Remineralization of Resin-Bonded Acid-Etched Dentin

Franklin R. Tay[1], David H. Pashley[2]

[1]Department of Endodontics, School of Dentistry, Medical College of Georgia, Augusta, Georgia, USA; [2]Department of Oral Biology, School of Dentistry, Medical College of Georgia, Augusta, Georgia, USA

*Correspondence: Dr. Franklin R. Tay, Department of Endodontics, School of Dentistry, Medical College of Georgia, Augusta, GA 30912-1129, USA. Tel: 706-721-2033, Fax: 706-721-6252, Email: FTAY@mcg.edu

Contemporary biomineralization strategies incorporate non-classical crystallization pathways of fluidic amorphous nanoprecursors and mesoscopic transformation. Using two functional biomimetic molecules, we previously regenerated mineralized dentin from acid-etched dentin using the Guided Tissue Remineralization (GTR) approach, with definitive intrafibrillar remineralization of type-I collagen. Degradation of denuded collagen within dentin adhesive resin-infiltrated dentin is a pertinent problem in dentin bonding. Here, we show that GTR provides a means of salvaging these degrading bonds by remineralizing resin-dentin interfaces. The GTR medium consists of a Portland cement/simulated body fluid that includes polyacrylic acid and polyvinylphosphonic acid biomimetic analogs for amorphous calcium phosphate dimension regulation and collagen targeting. Both interfibrillar and intrafibrillar apatites became readily discernible within the adhesive-bonded dentin after 2-4 months. Amorphous nanoprecursors created by GTR also penetrated the adhesive resin matrix to create nanocomposites. We anticipate GTR to be the starting point for more sophisticated strategies in extending the longevity of resin-dentin bonds.

INTRODUCTION

Guided Tissue Remineralization is a remineralization scheme that involves binding of biomimetic analogs to dentin collagen so that the doped collagen can guide the scale and distribution of remineralization[1]. For most vertebrates, collagen fibrils alone cannot initiate tissue mineralization. Other non-collagenous extracellular matrix (ECM) proteins derived from the secretory calcium-binding phosphoprotein (SCPP) family[2] are required for regulating bone and dentin mineralization and for controlling the dimension, order and hierarchy of carbonated apatite apposition within mineralized hard tissues[3,4]. As the use of native or recombinant ECM proteins[5,6] for in-situ biomineralization is not yet economically viable, scientists have resorted to the use of polyelectrolyte and poly(amino) acid macromolecules that mimic the functional domains of these natural proteins as alternative biomineralization strategies[7-9]. Biomimetics, however, must recapitulate the dimensions and order of mineral phases found in natural mineralized tissues[10,11]. Earlier collagen mineralization studies were based on the classical ion-mediated crystallization pathway[12,13], using metastable, supersaturated solutions or gels as diffusible sources of calcium and phosphate ions[14]. The biomimetic molecules were perceived to align around specific crystalline planes and act as inhibitors or promoters of crystal nucleation or growth[15]. While these studies were relatively successful in reducing the dimensions of calcium phosphate phases[16], they were unable to reproduce the order and hierarchy of apatite deposition (i.e. interfibrillar and intrafibrillar minerals) within the collagen matrix. The calcium phosphate depositions from these studies appeared more like surface dystrophic calcifications[17,18] than true intrafibrillar mineralization of collagen fibrils[6,19]. In particular, intrafibrillar mineralization has been suggested as the major contributor to the mechanical properties of mineralized dentin[19].

Failure of the classical crystallization theory to account for the diversity and complexity of

mineralization in exoskeletons has led to the identification of the contribution of metastable, fluidic amorphous mineral precursors in natural mineralization processes[20,21]. Initially reported in calcium carbonate mineralization systems[22], the involvement of amorphous calcium phosphate precursors[23] in biomineralization has recently been revived[24]. More recently, the contribution of a particle-mediated non-classical crystallization pathway to biomineralization has further been acknowledged[12,13]. In the presence of adequate calcium and phosphate ions, this pathway has been reported to be independent of ion solubility products, and relatively insensitive to changes in pH and osmolarity. In particle-mediated crystallization, inorganic nanocrystals stabilized by polymer molecules undergo self-assembly and crystallographic alignment to produce larger mesocrystals that function as intermediates prior to their transformation into single microscopic crystals.

Amorphous calcium phosphate is produced when Portland cement, a high pH, slow calcium- and silicon-releasing system comes into contact with a phosphate-containing medium[25]. With the advent of nanotechnology, amorphous calcium phosphate phases can be stabilized and reduced to a nanoscale using polyelectrolytes such as poly(acrylic) acids[26]. Using two separate biomimetic analogs to simulate the dual functions of dentin matrix protein 1 in calcium phosphate precursor stabilization and their targeting to collagen gap zones[5,27], we succeeded in regenerating mineralized dentin from partially-demineralized acid-etched dentin using Guided Tissue Remineralization[1]. As both intrafibrillar and interfibrillar minerals were present within the remineralized dentin type-I collagen, we have been able to recapitulate the dimension and order of the apatite crystallites that are found in natural intertubular dentin. To the best of our knowledge, this is the only ultrastructural evidence available in the biomineralization literature showing definitive intrafibrillar apatite remineralization of human type-I collagen.

A prospective translational application of Guided Tissue Remineralization is the adoption of the technique for perfecting the sealing qualities of resin-dentin bonds. Resin-dentin bonding is a unique form of tissue engineering in dentistry[28], in which a demineralized collagen matrix continuous with the underlying mineralized dentin is created by the use of acid-etching or acidic self-etching adhesives and is employed as the scaffold for resin infiltration. This layer of resin-infiltrated dentin (i.e. hybrid layer) provides the means for retention of tooth-colored resin-composite restorations when the overlying enamel layer is lost or absent. The most compelling problem currently associated with resin-dentin bonding is its poor durability, with billions of dental care dollars spent annually on replacement of these restorations. There are two major reasons for the poor durability of resin-dentin bonds. The first is increased water sorption by the hydrophilic resin components present in these adhesives[29]. Subsequent leaching of hydrolyzed resin components from these hydrophilic domains results in a porous adhesive with increased permeability. The second reason is the degeneration of collagen fibrils by endogenous matrix metalloproteinases (MMPs) in the hybrid layers of resin-bonded dentin[30]. Although degradation of denuded collagen matrices beneath imperfectly-created hybrid layers may be postponed by application of MMP inhibitors such as chlorhexidine as part of the dentin bonding procedures[31], a zone of resin-sparse, demineralized dentin inadvertently remains that is potentially susceptible to creep rupture[32] or cyclic fatigue rupture[33] during function.

Here, we explore the applicability of Guided Tissue Remineralization to adhesive dentistry as a means of remineralizing incompletely-infiltrated resin-dentin interfaces created by two commercially available simplified etch-and-rinse adhesives, One-Step and Single Bond Plus. The remineralization medium consists of a set Portland cement/simulated body fluid system containing polyacrylic acid and polyvinylphosphonic acid as biomimetic analogs. Within 2-4

months, areas within the hybrid layers that are initially poorly infiltrated by adhesive resins are remineralized to the extent that they appear similar in ultrastructure as the underlying mineralized intertubular dentin. Areas that are better infiltrated with resin are not remineralized. Surprisingly, we also observed heterogeneous deposition of apatite nanoclusters within potentially porous regions of the adhesive layer that are vulnerable to water entrapment during the initial bonding procedure.

RESULTS

Control specimens

We confirmed that remineralization of resin-dentin interfaces occurred only under the conditions of Guided Tissue Remineralization by examining control specimens bonded with One-Step (Fig. 1a) or Single Bond Plus (Fig. 1e) using transmission electron microscopy of unstained, non-demineralized sections. These specimens were immersed for up to 4 months in a control Portland cement/ simulated body fluid system which did not contain biomimetic analogs. Specimens retrieved after 4 months revealed the absence of remineralization within the hybrid layers. Selected Area Electron Diffraction (SAED) of the mineralized dentin base (Fig. 1b) revealed concentric rings that are characteristic of small crystalline aggregates. The two most prominent rings represent the 002 and 211 planes of apatite[34]. A ring-less diffuse diffraction pattern was seen in the hybrid layer (not shown).

We also immersed our control specimens in 50 wt% ammoniacal silver nitrate. The silver nitrate diffuses into any water-filled voids. As the diamine silver ions are reduced to silver after light exposure, regions of incomplete resin infiltration (nanoleakage) within the hybrid layers and potential voids within the adhesive layers can be readily discerned as streaks or isolated grains of silver deposits[35]. Figure 1c represents nanoleakage present in One-Step-bonded dentin

after 4 months of immersion in the control medium. Nanoleakage can be seen within the top and middle portion of the hybrid layer, while the bottom of the hybrid layer is better infiltrated by the adhesive resin. Figure 1d represents the junction between the adhesive and resin-composite. Numerous isolated silver grains can be identified. They represent a potentially porous region in the adhesive in which water eluting from the dentin surface was trapped by light-curing of the adhesive[36]. Figure 1f represents a Single Bond Plus specimen showing nanoleakage within the hybrid layer as well as silver-filled water channels (i.e. water trees)[36] within the filled adhesive layer. Taken together, the data derived from the control specimens indicate that potentially porous regions are present within the adhesive layer and hybrid layer of both adhesives that are amendable to Guided Tissue Remineralization.

Experimental Specimens

Specimens bonded with the two adhesives were retrieved after 1-4 months of Guided Tissue Remineralization and examined using transmission electron microscopy. Remineralization of the resin-dentin interfaces should be perceived as a continuum of events. However, for narrative purpose, they are presented as four separate stages with the most probable time scale of occurrence of each stage included in parentheses:

A) Stage I – Amorphous Precursor Stage (1 month);

B) Stage II – Interfibrillar Remineralization Stage (1-2 months);

C) Stage III – Intrafibrillar Remineralization Stage (2-3 months); and

D) Stage IV – Equilibrium Stage (3-4 months).

Ultrastructural changes that occurred at Stage I (Amorphous Precursor Stage) were subtle and not discernable below 5000X magnification. Figure 2a represents a specimen retrieved after one month of Guided Tissue Remineralization, showing unusual electron densities along the

interfibrillar spaces of the hybrid layer. A higher magnification view (Fig. 2b) revealed electron-dense, amorphous structures that probably represent coalesced fluidic amorphous calcium phosphate nanoprecursors that had penetrated the incompletely infiltrated regions of the hybrid layer. Selected area electron diffraction of these amorphous structures resulted in a broad, diffuse pattern without concentric rings (Fig. 2c), indicating their non-crystalline status.

Stage II (Interfibrillar Remineralization Stage) is represented by the appearance of nanocrystals within the interfibrillar spaces of the hybrid layer (Fig. 2d). Initially (after 1 month), these nanocrystals were much finer than the apatite platelets from the underlying mineralized dentin base (Fig. 2e). They probably represent polymer-stabilized mesocrystalline apatite phases[1] that eventually undergo mesoscopic assembly and transformation[12,13] into larger needle-shaped crystallites (*ca*. 20 nm long) within the interfibrillar spaces (Fig. 2f).

Stage III (Intrafibrillar Remineralization Stage) can be readily identified by TEM at lower magnifications (Fig. 3a) after 2-3 months of Guided Tissue Remineralization. The earliest evidence of intrafibrillar remineralization may be depicted as an ordered alignment of nanocrystals within the collagen fibril. These intrafibrillar nanocrystals co-exist with adjacent interfibrillar nanocrystals (Fig. 3b), both of which appeared much smaller than the intrafibrillar and interfibrillar apatite platelets seen in mineralized intertubular dentin. A more advanced stage of Intrafibrillar Remineralization Stage (after 3 months of Guided Tissue Remineralization) is depicted in Figure 3c. Remineralized regions within the hybrid layers could be readily discerned from those non-remineralized, better resin-infiltrated regions. At a high magnification (Fig. 3d), mesoscopic transformation of the original nanocrystals had probably occurred, with the larger crystallite platelets (*ca*. 20 nm long) stacked in a repeating and orderly sequence within the collagen fibrils (*ca*. 100 nm in diameter). The crystallographic c-axes of these electron-dense

platelets were well aligned with the longitudinal axis of the collagen fibrils, thereby producing the arc-shaped SAED diffraction patterns[34,37] along the (002) plane of apatite (Fig. 3e). Longer needle-shaped crystallites (*ca*. 50 nm along the c-axis) could also be seen along the periphery of the fibrils (i.e. interfibrillar remineralization), although they were sparse and did not cover the entire fibril. Along the surface of the hybrid layer, collagen fibrils that were previously completely demineralized are shown extending into the overlying adhesive layer. They were heavily remineralized and exhibited a dense array of apatite platelets (Fig. 3f).

Stage IV (Equilibrium Stage) represents an advanced stage of Guided Tissue Remineralization wherein the extent of remineralization within the hybrid layers had reached a state of equilibrium and would not be expected to exhibit further improvements. Figures 4a and 4b represent resin-dentin interfaces bonded with the water-free, acetone-based One-Step adhesive and retrieved after three and four months of Guided Tissue Remineralization, respectively. For both specimens, extensive remineralization had occurred in the top and middle parts of the hybrid layer. The base of the hybrid layers did not remineralize irrespective of the time of immersion of the specimens in the remineralization medium. This suggested that the base of the hybrid layers in One-Step is better resin-infiltrated than the top and middle portions. At this stage, although intrafibrillar remineralization could still be recognized by the banded appearance in some of the collagen fibrils, it has largely been masked by more extensive interfibrillar mineral deposits (Fig. 4c). These heavily remineralized regions revealed SAED ring patterns that are devoid of arc-shaped patterns (Fig. 4d), suggesting a more random crystallite arrangement contributed by the more extensive interfibrillar remineralization (see also Fig. 1b). The ethanol-based, water-containing adhesive Single Bond Plus produced a different Stage IV remineralization pattern (Figs. 4e), wherein extensive remineralization occurred within the

middle and base of the hybrid layer. The surface 1-2 μm of the hybrid layer appeared to be better infiltrated by the filled adhesive and was not remineralized (Fig. 4f).

A rather surprising finding was that during the process of Guided Tissue Remineralization, apatite nanocomposites were created within the potentially porous adhesive layers, as already illustrated in Figures 2d, 4a and 4b. Apatite deposition within the unfilled polymer matrix of the One-Step adhesive was heterogeneous; the two predominant sites of deposition being the water-rich channels (water trees) close to the dentin surface (Fig. 5a) where porous regions within the adhesive were filled with bundles of co-aligned crystalline filaments[38] (Fig. 5b). The other site of nanocomposite formation is a water-rich zone directly beneath the resin composite (Fig. 5c). The latter was caused by the entrapment of water that was thermally expressed from the resin-dentin interface as the adhesive layer was light-cured (see nanoleakage results in Fig. 1d). The thickness and density of this nanocomposite zone increased with the time of immersion in the Guided Tissue Remineralization medium (Fig. 5d). Nanocomposite formation in the Single-Bond Plus adhesive was difficult to discern, as nanofillers were present in this filled adhesive. Nevertheless, water trees that originated from the surface of the hybrid layer were filled with minerals after Guided Tissue Remineralization (Fig. 5e). Similar to the silver nanoleakage observed in the control specimens (Fig. 1f), these mineral-filled water trees (pointer) extended through the entire adhesive layer (Fig. 5f).

Cryofractured resin-dentin interfaces

The TEM results obtained from epoxy resin-embedded specimens were also confirmed with field emission-scanning electron microscopy (FE-SEM) of non-resin-embedded, cryofractured resin-dentin interfaces. Unlike the use of TEM, it is impossible to identify the type of adhesive employed based on SEM examination. However, the results are generically

applicable to both adhesives. Figure 6a represents a control specimen that had been immersed in Portland cement/simulated body fluid (with biomimetic analogs) for 4 months. The incompletely resin-infiltrated zone at the base of the hybrid layer contains denuded, demineralized collagen fibrils that appear smooth and shrunken after dehydration (Fig. 6b), indicating that they were devoid of supporting intrafibrillar or interfibrillar minerals. By contrast, in experimental specimens that had undergone Guided Tissue Remineralization for only 2 months (Fig. 6c), some of the collagen fibrils exhibited a "corn-on-the cob" appearance[1] that is suggestive of interfibrillar remineralization. After 4 months of Guided Tissue Remineralization, most of the collagen fibrils from the originally denuded collagen matrix had either a "corn-on-the-cob" appearance or appeared swollen and vaguely banded (Fig. 6D). The latter is indicative of the presence of intrafibrillar supporting minerals that resist dehydration shrinkage of the fibrils.

DISCUSSION

We have previously demonstrated that reducing the dimension of amorphous calcium phosphate precursors (ca. 200-500 nm) to a nanoscale (< 50 nm) may be achieved using poly(acrylic) acid or poly(aspartic) acid, and that the use of additional analogs to simulate ECM phosphoproteins is not necessary for this initial phase of Guided Tissue Remineralization[1]. Figure 7a is a schematic representing the penetration of polyacrylic acid-stabilized amorphous calcium phosphate nanoprecursors into the hybrid layer via the resin-sparse, collagen rich regions as well as potentially porous regions within the adhesive layer.

Figure 7b is a schematic representation of Stage I of Guided Tissue Remineralization. We perceive that the amorphous nanoprecursors could have easily penetrated the poorly resin-infiltrated parts of the hybrid layer where the interfibrillar spaces are exposed. As these 20 nm

wide interfibrillar spaces are extremely tortuous, they could have served as a template for molding and coalescence of the fluidic amorphous nanoprecursors, in a way that is analogous to the creation of single calcite superstructures (e.g. sea urchin spine) with indiscriminate crystalline planes and curved morphologies[24,39,40]. The presumably liquid-like nature of polymer-stabilized amorphous precursors has been referred to as "polymer-induced liquid-precursors (PILPs)"[41], although direct proof that these droplets are indeed liquid is unavailable[42]. It is also amazing how mineral deposition could have occurred within the adhesive layer resulting in the formation of nanocomposites. Although the occurrence of silver nanoleakage within the adhesive (Fig. 1d) implies that silver can be deposited as a mineral within the polymer matrix, the ionic radius of the silver ion (115 pm) is much smaller when compared to that of the amorphous calcium phosphate nanoprecursor. Thus, the fluidic nature of these amorphous nanoprecursors provided a plausible explanation on how they could have followed the pathways of water movement within the polymerized adhesive[43] and penetrated the water-filled nanovoids within the adhesive layer.

Figure 7c is a schematic depicting the second stage of Interfibrillar Remineralization within a poorly infiltrated region of the hybrid layer. We hypothesize that the polyvinylphosphonic acid-containing analog molecules that diffuse into the denuded collagen matrix are bound initially to specific sites along the surface of the collagen fibrils. This is analogous to the attachment of different ECM phosphoprotein molecules to specific collagen binding sites[44,45]. Auto-transformation of the coalesced amorphous calcium phosphate nanoprecursors into apatite results in their deposition within the interfibrillar spaces. Figure 7d is a schematic depicting the third stage of Intrafibrillar Remineralization within a poorly resin-infiltrated region of the hybrid layer. We speculate that the polyvinylphosphonic acid-containing

molecules diffuse into the collagen fibrils and attach to the specific locations along the tropocollagen molecules, thereby guiding mineral deposition within the gap regions of the collagen fibrils[46]. The initially formed nanocrystals (Fig. 3b) are smaller than the dimensions of the intrafibrillar apatite platelets (Fig. 3d). Thus, we further hypothesize that the single-crystal apatites platelets represent the end products of mesoscopic transformation of multiple, orderly arranged and closely approximated polyacrylic acid-stabilized mesocrystalline intermediates. This bricklaying, "Lego-like" modular assembly strategy through a particle-mediated approach[42] probably proceeds via the formation of nanoscopical mineral bridges across the surfaces of the mesocrystals[47]. Thus, with the use of two biomimetic analogs that are designed for different functions, we verified that the "bottom-up" particle-mediated crystallization pathway[48] does not only exist in theory, but indeed permits hierarchical crystalline order (i.e. intrafibrillar and interfibrillar minerals) to be re-established in resin-contaminated dentin type-I collagen fibrils under ambient temperature. These remarkable features have never been demonstrated using traditional technology of crystal growth that focused on the "top-down" fabrication of homogeneous, large-size single crystals[48].

The so-called "Equilibrium Stage" of Guided Tissue Remineralization is a rather philosophical concept that requires further elaboration. Although the One-Step adhesive demonstrated a general trend of better infiltration at the base of the hybrid layers, one can clearly see in Fig. 4a that the left side of the specimen is more profusely remineralized than the right side, suggesting that the specimen was initially better infiltrated by resin on the right side. Based on these results, one would expect that two vertical nanoindentation lines performed across the left and right sides of remineralized hybrid layers will produce different results in terms of the changes in mechanical properties such as elastic modulus and hardness within the hybrid layer.

Indeed, the extent of remineralization is dependent upon the initial status of resin infiltration (Fig. 5a *vs* Fig. 5b) and was found to vary considerably from specimen to specimen and from location to location. Based on these important ultrastructural results, we have learnt that reports on changes in mechanical properties as discrete value sets would not be sufficient to represent the complexity and variation of remineralized hybrid layers. Rather, a mapping correlating the variation in mechanical properties with ultrastructural changes for a particular specimen would be a more appropriate alternative.

In summary, this report provides proof-of-concept that resin-dentin interfaces created by contemporary dentin adhesives are permeable to polyelectrolyte-stabilized amorphous calcium phosphate nanoprecursors and that "resin-contaminated" collagen can be remineralized via the guidance of a phosphoprotein-mimicking biomimetic analog as long as these fibrils remain structurally intact. The current Guided Tissue Remineralization model laid the foundation for more sophisticated strategies to be designed for extending the longevity of resin-dentin bonds. For example, in the current model, each resin-dentin slab is placed sideway on top of a set Portland cement block, with the contact surface rotated every fortnight. This strategy is not possible clinically and delivery systems that incorporate set Portland cement particles in either the adhesive or restorative material have to be considered for remineralization to proceed from the top of the adhesive-bonded dentin to the mineralized dentin base via diffusion of the amorphous calcium phosphate nanoprecursors. Moreover, additional strategies have to be considered for incorporating the biomimetic analogs as part of the delivery systems. Our preliminary work indicates that it is possible to include up to 5 mass% of a solution of these analogs as part of an experimental adhesive formulation, without creating visibly-discernible, gross phase separation within the adhesive. Conversely, nano-phase separation of the aqueous

solution within the adhesive resin matrix may provide a means for coaxing these biomimetic analogs into the hybrid layer. Investigations on these techniques are in order to put this particle-mediated remineralization technology into clinical use.

METHODS

Dentin Bonding Procedures

Twenty recently extracted human third molars were collected after patients' informed consent were obtained under a protocol reviewed and approved by the Human Assurance Committee of the Medical College of Georgia. A flat dentin surface was prepared perpendicular to the longitudinal axis of each tooth using a slow-speed Isomet diamond saw (Buehler Ltd) under water-cooling. The occlusal dentin surface was polished with a 400-grit silicon carbide paper attached to an Ecomet III variable speed grinder-polisher (Buehler Ltd.) under running water to create a bonding surface in mid-coronal dentin that was devoid of enamel and contained a standardized smear layer. Two simplified etch-and-rinse dentin adhesives were used: One-Step (Bisco Inc.), a water-free, acetone-based unfilled adhesive, and Single Bond Plus (3M ESPE), a water-containing, ethanol-based filled adhesive. Ten teeth were randomly assigned to each adhesive. Each dentin surface to be bonded was etched with a 32% phosphoric acid gel (Uni-Etch, Bisco, Inc.) for 15 sec to create a 5-8 µm thick zone of completely demineralized dentin on top of a mineralized dentin base. The etched dentin surface was thoroughly rinsed with deionized water, and bonded with the respective adhesive using a moist bonding technique by keeping the etched dentin visibly moist during bonding. After evaporation of the adhesive solvent, each adhesive was polymerized for 20 sec using a quartz-tungsten-halogen light-curing unit with an output intensity of 600 mW/cm^2. This was followed by incremental placement of two 2-mm thick layers of a resin composite that was light-cured separately for 40 sec. Each tooth was then

sectioned occluso-gingivally into 1-mm thick slabs, each containing the resin-dentin interface in the center of the slab.

Preparation of Portland cement

Type I white Portland cement (Lehigh Cement Company) was sieved and mixed with deionised water in a water-to-powder ratio of 0.35:1, placed in flexible silicone molds and allowed to set and age at 100% relative humidity for one month before use.[1] Leaching of the calcium hydroxide from the set Portland cement provides the source of calcium and hydroxyl ions for the precipitation of calcium deficient apatite via an initial amorphous calcium phosphate phase when the cement comes into contact with phosphate ions[25].

Simulated Body Fluid and Biomimetic Analogs

Glasswares were rinsed with a solution of chromium trioxide and sulphuric acid, three times with deionised water, followed by acetone and left to oven-dry before use. A simulated body fluid was prepared by dissolving 136.8 mM NaCl, 4.2 mM $NaHCO_3$, 3.0 mM KCl, 1.0 mM $K_2HPO_4 \cdot 3H_2O$, 1.5 mM $MgCl_2 \cdot 6H_2O$, 2.5 mM $CaCl_2$ and 0.5 mM Na_2SO_4 in deionized water[49] and adding 3.08 mM sodium azide to prevent bacterial growth. The simulated body fluid was buffered to pH 7.4 with 0.1 M Tris Base and 0.1 M HCl and filtered. For Guided Tissue Remineralization, 500 μg/mL of polyacrylic acid (Sigma-Aldrich; MW 1800) and 200 μg/mL of polyvinylphosphonic acid (Sigma-Aldrich; MW 62000) were added to the simulated body fluid as biomimetic analogs. The pH of the remineralization medium was similarly adjusted to 7.4.

Guided Tissue Remineralization

Each experimental specimen slab was placed on top of a set Portland cement block (ca. 1 g) inside a glass scintillation vial. The latter was filled with 15 mL of simulated boy fluid

containing the two biomimetic analogs. The setup for the control specimens was the same, except that the liquid medium was replaced with simulated body fluid that did not contain biomimetic analogs. Each glass vial was capped to prevent evaporation of the solution and stored in an incubator at 37 °C. As only one side of the specimen was in contact with the Portland cement block, each specimen was turned once every two weeks to ensure that the other side of the specimen slab was also in contact with the cement block. Experimental specimens were retrieved after 1, 2 3 and 4 months (N=5) for ultrastructural examination of the extent of remineralization. Control specimens were examined at the baseline period (i.e. before immersion) and after 4 months of immersion in the Portland cement/simulated body fluid.

Transmission Electron Microscopy

Following retrieval from the respective solution, the specimen slices were fixed in Karnovsky's fixative, rinsed in cacodylate buffer, post-fixed in 1% osmium tetroxide, and further rinsed three times in cacodylate buffer. They were dehydrated in an ascending series of ethanol (50-100%), immersed in propylene oxide as a transitional fluid and subsequently embedded in epoxy resin. Non-demineralized, epoxy resin-embedded, 70-90 nm thick sections were prepared and examined without further staining using a the JEM-1230 transmission electron microscope (JEOL) operated at 80 kV.

For the control group, two additional specimens were immersed in 50 wt% ammoniacal silver nitrate for silver nanoleakage examination within the dentin hybrid layers, according to our previously reported protocol[35]. After reduction of the diamine silver ions into metallic silver, the specimens were processed and examined in the manner described above.

Scanning Electron Microscopy

To facilitate cryofracture, slits were cut into the composite and the dentin side of each slab but without extending into the resin-dentin interface. Each slab was immersed in liquid nitrogen for 2 min and dropped into deionized water. Expansion of the ice within the water-filled slit resulted in spontaneous splitting of the slab into two halves. The cryofractured specimens were dehydrated in an ascending series of ethanol (50-100%), and immersed in hexamethyldisilasane[50] that was allowed to evaporate slowly during the final chemical dehydration step. The specimens were sputter-coated with gold/palladium and examined along their fractured edges using a XL-30 field emission-scanning electron microscope (Philips) operated at 5 kV.

ACKNOWLEDGEMENTS

This study was supported by the Medical College of Georgia's Dental Research Center. We thank Bob Smith for TEM technical assistance and Michelle Barnes for secretarial support.

COMPETING INTEREST STATEMENT

The authors declare that they have no competing financial interests.

REFERENCES

1. Tay, F.R. & Pashley, D.H. Guided tissue remineralisation of partially demineralised human dentine. *Biomaterials* **29**, 1127–1137 (2008).
2. Kawasaki, K. & Weiss, K.M. Evolutionary genetics of vertebrate tissue mineralization: the origin and evolution of the secretory calcium-binding phosphoprotein family. *J. Exp. Zoolog. B Mol. Dev. Evol.* **306**, 295–316 (2006).
3. Traub, W., Arad, T. & Weiner, S. Three-dimensional ordered distribution of crystals in turkey tendon collagen fibers. *Proc. Natl. Acad. Sci. U.S.A.* 86, 9822–9826 (1989).
4. Gajjeraman, S., Narayanan, K., Hao, J., Qin, C. & George, A. Matrix macromolecules in hard tissues control the nucleation and hierarchical assembly of hydroxyapatite. *J. Biol. Chem.* **282**, 1193–1204 (2007).
5. He, G. *et al*. Spatially and temporally controlled biomineralization is facilitated by interaction between self-assembled dentin matrix protein 1 and calcium phosphate nuclei in solution. *Biochemistry* **44**, 16140–16148 (2005).
6. Wazen, R.M. *et al*. In vivo functional analysis of polyglutamic acid domains in recombinant bone sialoprotein. *J. Histochem. Cytochem.* **55**, 35–42 (2007).
7. Tsortos, A. & Nancollas, G.H. The role of polycarboxylic acids in calcium phosphate mineralization. *J. Colloid. Interface. Sci.* **250**, 159–167 (2002).
8. Girija, E.K., Yokogawa, Y. & Nagata, F. Apatite formation on collagen fibrils in the presence of polyacrylic acid. *J. Mater. Sci.: Mater. Med.* **15**, 593–599 (2004).
9. Schweizer, S. & Taubert, A. Polymer-controlled, bio-inspired calcium phosphate mineralization from aqueous solution. *Macromol. Biosci.* **7**, 1085–1099 (2007).
10. Sanchez, C., Arribart, H. & Guille, M.M. Biomimetism and bioinspiration as tools for the

design of innovative materials and systems. *Nat. Mater.* **4**, 277–288 (2005).

11. Weiner, S. Biomineralization: A structural perspective. *J. Struct. Biol.* [Epub ahead of print] (2008).

12. Niederberger, M. & Cölfen, H. Oriented attachment and mesocrystals: non-classical crystallization mechanisms based on nanoparticle assembly. *Phys. Chem. Chem. Phys.* **8**, 3271–3287 (2006).

13. Xu, A-W., Ma, Y. & Cölfen, H. Biomimetic mineralization. *J. Mater. Chem.* **17**, 415–449 (2007).

14. Silverman, L. & Boskey, A.L. Diffusion systems for evaluation of biomineralization. *Calcif. Tissue. Int.* **75**, 494–501 (2005).

15. Boskey, A.L. Biomineralization: an overview. *Connect. Tissue. Res.* **44** (Suppl 1), 5–9 (2003).

16. Boanini, E., Torricelli, P., Gazzano, M., Giardino, R. & Bigi, A. Nanocomposites of hydroxyapatite with aspartic acid and glutamic acid and their interaction with osteoblast-like cells. *Biomaterials* **27**, 4429–4433 (2006).

17. Bradt, J-H., Mertig, M., Teresiak, A. & Pompe, W. Biomimetic mineralization of collagen by combined fibril assembly and calcium phosphate formation. *Chem. Mater.* **11**, 2694–2701 (1999).

18. Li, X. & Chang, J. Preparation of bone-like apatite-collagen nanocomposites by a biomimetic process with phosphorylated collagen. *J. Biomed. Mater. Res. A.* **85**, 293–300 (2008).

19. Kinney, J.H., Habelitz, S., Marshall, S.J. & Marshall, G.W. The importance of intrafibrillar mineralization of collagen on the mechanical properties of dentin. *J. Dent. Res.* **82,** 957–

961 (2003).

20. Weiner, S., Sagi, I. & Addadi, L. Structural biology. Choosing the crystallization path less traveled. *Science* **309**, 1027-1028 (2005).

21. Olszta, M.J., Odom, D.J., Douglas, E.P. & Gower, L.B. A new paradigm for biomineral formation: mineralization via an amorphous liquid-phase precursor. *Connect. Tissue Res.* **44** (Suppl 1), 326–334 (2003).

22. Politi, Y., Arad, T., Klein, E., Weiner, S. & Addadi, L. Sea urchin spine calcite forms via a transient amorphous calcium carbonate phase. *Science* **306**, 1161–1164 (2004).

23. Eanes, E.D. Amorphous calcium phosphate. *Monogr. Oral. Sci.* **18**, 130–147 (2001).

24. Cölfen, H. Single crystals with complex form via amorphous precursors. *Angew. Chem. Int. Ed. Engl.* **13**, 2351–2353 (2008).

25. Tay, F.R., Pashley, D.H., Rueggeberg, F.A., Loushine, R.J. & Weller, R.N. Calcium phosphate phase transformation produced by interaction of the Portland cement component of white MTA with a phosphate-containing fluid. *J. Endod.* **33**, 1347-1351 (2007).

26. Liou, S.C., Chen, S.Y. & Liu, D.M. Manipulation of nanoneedle and nanosphere apatite/poly(acrylic acid) nanocomposites. *J. Biomed. Mater. Res. B Appl. Biomater.* **73**, 117–122 (2005).

27. He, G., Dahl, T., Veis, A. & George, A. Nucleation of apatite crystals in vitro by self-assembled dentin matrix protein 1. *Nat. Mater.* **2**, 552–558 (2003).

28. Tay, F.R. & Pashley, D.H. Dental adhesives of the future. *J. Adhes. Dent*. **4**, 91–103 (2002).

29. Ito, S. *et al.* Effects of resin hydrophilicity on water sorption and changes in modulus of elasticity. *Biomaterials* **26**, 6449–6459 (2005).

30. Pashley, D.H. *et al.* Collagen degradation by host-derived enzymes during aging. *J. Dent. Res.* **83**, 216–221 (2004).

31. Carrilho, M.R.O. *et al*. *In vivo* preservation of the hybrid layer by chlorhexidine. *J. Dent. Res.* **86**, 529–533 (2007).

32. Wang, X.T. & Ker, R.F. Creep rupture of wallaby tail tendons. *J. Exp. Biol.* **198** (Pt 3), 831–845 (1995).

33. Wang, X.T., Ker, R.F. & Alexander, R.M. Fatigue rupture of wallaby tail tendons. *J. Exp. Biol.* **198** (Pt 3), 847–852 (1995).

34. Müller, F.A., Müller, L., Caillard, D. & Conforto, E. Preferred growth orientation of biomimetic apatite crystals. *J. Crystal Growth* **304**, 464–471 (2007).

35. Tay, F.R., Pashley, D.H. & Yoshiyama, M. Two modes of nanoleakage expression in single-step adhesives. *J. Dent. Res.* **81**, 472–476 (2002).

36. Tay, F.R., Pashley, D.H., Suh, B.I., Hiraishi, N. & Yiu, C.K. Water treeing in simplified dentin adhesives--déjà vu? *Oper. Dent.* **30**, 561–579 (2005).

37. Mishima, H. & Sakae, T. Demonstration of strucgtural variation in rat incisor dentin as determined by the X-ray Laue method. *J. Dent. Res.* **65**, 932–934 (1986).

38. Fowler, C.E., Li, M., Mann, S. & Margolis, H.C. Influence of surfactant assembly on the formation of calcium phosphate materials – A model for dental enamel formation. *J. Mater. Chem.* **15**, 3317–3325 (2005).

39. Meldrum, F.C. & Ludwigs, S. Template-directed control of crystal morphologies. *Macromol. Biosci*. **7,** 152–162 (2007).

40. Kulak, A.N. *et al*. Continuous structural evolution of calcium carbonate particles: a unifying model of copolymer-mediated crystallization. *J. Am. Chem. Soc.* **129**, 3729–3736

(2007).

41. Gower L. A. & Tirrell, D. A. Calcium carbonate films and helices grown in solutions of poly(aspartate) – Chemical and Biochemical Perspectives. *J. Crystal Growth* **191**, 153–160 (1998).

42. Cölfen H. Bio-inspired mineralization using hydrophilic polymers. *Top. Curr. Chem.* **271**, 1–77 (2007).

43. Tay *et al*. Single-bottle adhesives behave as permeable membranes after polymerization. I. *In vivo* evidence. *J. Dent.* **32**, 611–621 (2004).

44. Dahl, T., Sabsay, B. & Veis, A. Type I collagen-phosphophoryn interactions: specificity of the monomer-monomer binding. *J. Struct. Biol*. **123**, 162–168 (1998).

45. He, G. & George, A. Dentin matrix protein 1 immobilized on type I collagen fibrils facilitates apatite deposition in vitro*. J. Biol. Chem*. **279**, 11649–11656 (2004).

46. Traub, W., Jodaikin, A., Arad, T., Veis, A. & Sabsay, B. Dentin phosphophoryn binding to collagen fibrils. *Matrix* **12**, 197–201 (1992).

47. Oaki, Y., Kotachi, A., Miura, T. & Imai, H. Bridged nanocrystals in biominerals and their biomimetics: classical yet modern crystal growth on the nanoscale. *Adv. Func. Mater*. **16**, 1633–1639 (2006).

48. Imai, H. Self-organized formation of hierarchical structures. *Top. Curr. Chem*. **270**, 43–72 (2007).

49. Kokubo, T., Kushitani, H., Sakka, S., Kitsugi, T. & Yamamuro, T. Solutions able to reproduce *in vivo* surface-structure changes in bioactive glass-ceramic A-W. *J. Biomed. Mater. Res.* **24**, 721–734 (1990).

50. Braet, F., De Zanger, R. & Wisse, E. Drying cells for SEM, AFM and TEM by

hexamethyldisilazane: a study on hepatic endothelial cells. *J. Microsc*. **186**(Pt 1), 84–87 (1997).

LEGEND OF FIGURES

Generic abbreviations applicable to all figures - C: composite; A: unfilled adhesive; FA: filled adhesive; H: hybrid layer; D: mineralized dentin.

Fig.1 TEM micrographs depicting the ultrastructure and silver nanoleakage of control specimens that have been stored in phosphate-containing fluid (containing Portland cement blocks but without biomimetic analogs) for 4 months. **a**. A One-Step specimen with a 5-8 µm thick hybrid layer that was completely devoid of apatite minerals. **b**. Electron diffraction of the mineralized dentin base beneath the hybrid layer revealed concentric rings (major *hkl* plane indices included) that are characteristic of small crystalline aggregates. The two most prominent rings (asterisks) represent the 002 plane and the closed approximated 211, 112, 300 and 202 planes of apatites. **c**. Silver permeation into water-filled interfibrillar spaces (pointer) identified from the hybrid layer of a specimen bonded with One-Step. **d**. Leaching of resinous components from a water-rich zone beneath the resin composite resulted in the manifestation of multiple isolated silver grains (open arrowhead) within the unfilled adhesive. **e**. A Single Bond Plus specimen revealed a completely demineralized hybrid layer with a similar thickness range (i.e. 5-8 µm). P: polyalkenoic acid copolymer component of the filled adhesive. **F**. Silver uptake (nanoleakage) in a Single Bond Plus specimen. Pointer: nanoleakage within hybrid layer; Open arrowheads: silver-filled water channels (i.e. water trees) within the filled adhesive layer. Large (3-4 µm diameter) silver deposits were water droplets in the adhesive layer.

Fig.2 Experimental specimens that have undergone Guided Tissue Remineralization (GTR) for 1-2 months revealed two subtle stages of remineralization within hybrid layers. Stage I, A-C. (**Amorphous Precursor Stage**); Stage II, D-F (**Interfibrillar Remineralization Stage**). **a**. A

One-Step specimen, taken at one month after GTR, showing interfibrillar spaces containing amorphous electron-dense structures (open arrowheads) in the hybrid layer. **b**. High magnification view of Fig. 2a showing the amorphous nature of the electron-dense structures (open arrowheads). They probably represent coalesced fluidic amorphous calcium phosphate nanoprecursors (pointer) that had penetrated the incompletely infiltrated regions of the hybrid layer. **c**. SAED of these amorphous structures resulted in a broad, diffuse pattern without concentric rings. **d**. A One-Step specimen, taken 2 months after GTR, showing the presence of very fine needle-shaped nanocrystals (open arrowheads) within interfibrillar spaces of the hybrid layer. These initially formed nanocrystals were smaller than the apatites that are found in natural mineralized dentin. Fine mineral deposits could also be identified with the adhesive layer (asterisk). The creation of "nanocomposite" in the adhesive layer via GTR is illustrated in detail in Figure 5. **e**. A Single Bond Plus specimen, taken 2 months after GTR, showing evidence of similar Stage II remineralization (open arrowheads) at the base of the hybrid layer. **f**. A high magnification view of Fig. 2E crystallites with the interfibrillar spaces of a collagen fibril (between open arrows). Needle-shaped crystallites (ca. 20 nm long) appeared to have been produced by the fusion of nanocrystals (open arrowhead).

Fig.3 TEM micrographs showing examples of Stage III (**Intrafibrillar Remineralization Stage**) in resin-dentin interfaces after 2-3 months of Guided Tissue Remineralization (GTR). **a**. A One-Step specimen taken after 2 months of GTR, with remineralization (pointer) observable at low magnification. **b**. High magnification of Fig. 3A, showing nanocrystals along the interfibrillar spaces (between open arrows). The earliest stage of intrafibrillar remineralization could be recognized as an ordered alignment of nanocrystals (open arrowheads). **c**. A One-Step specimen taken after 3 months of GTR with remineralization occurring in the middle of the

hybrid layer and along the surface collagen fibrils (arrow). Regions that were not remineralized (asterisks) were probably better infiltrated with adhesive resin. **d**. A high magnification view of the region depicted by the “pointer” in Fig. 3c, illustrating a more advanced stage of intrafibrillar remineralization. Crystallite platelets (ca. 20 nm long) were stacked in a repeating and orderly sequence (triple open arrowheads) within the collagen fibrils (ca. 100 nm in diameter). The crystallographic c-axes of these electron-dense platelets were well aligned with the axis of the collagen fibrils. Larger needle-shaped crystallites (ca. 50 nm) could be seen (pointers) along the periphery of the fibrils (i.e. interfibrillar remineralization). **E**. SAED of the region in Fig. 3d. The arc-shaped diffraction patterns ascribed to the (002) plane of apatite suggests that the c-axes of the platelets have a preferential orientation. **F**. A high magnification view of Fig. 3c showing the density of apatite platelets within a remineralizsed collagen fibril (arrow) along hybrid layer surface.

Fig.4 TEM micrographs showing examples of Stage IV remineralization (**Equilibrium Stage**) in resin-dentin interfaces that have undergone 3-4 months of GTR. **a**. A One-Step specimen with extensive remineralization of the top and middle parts of the hybrid layer (asterisk). The base of the hybrid layer appeared to be better infiltrated and did not remineralize. Initial evidence of mineralization of the adhesive layer could be seen as an electron-dense band (pointer) beneath the composite (see Fig. 5 for details). **b**. Another One-Step specimen with even more profuse remineralization of the hybrid layer (asterisk). Extensive mineralization of the adhesive layer could also be seen (star). **c**. High magnification of the heavily remineralized regions. Intrafibrillar remineralization could be recognized by the banded appearance of the collagen fibrils (open arrowheads), although this feature has largely been masked by heavy interfibrillar minerals. **d**. SAED of these heavily remineralized regions revealed diffraction rings that are

ascribed to the major 002 and 211 planes of apatites. Absence of arc-shaped patterns in the 002 ring suggests a more random, overall crystallite arrangement. **e.** A Single Bond Plus specimen showing extensive remineralization within the middle and base of the hybrid layer (R). The total thickness of the hybrid layer is depicted by the two open arrows. The surface 2 µm of the hybrid layer (asterisk) appeared to be better infiltrated by the filled adhesive and did not remineralize. **f**. High magnification of Fig.4E showing the absence of remineralization (between open arrowheads) from the surface of the hybrid layer.

Fig.5 During Guided Tissue Remineralization, apatite nanocomposites were unexpectedly created within the potentially porous adhesive layers. Apatite deposition within the polymer matrix was heterogeneous; the two predominant sites of deposition being the water-rich channels (water trees) close to the dentin surface and a water-rich zone directly beneath the resin composite (see nanoleakage results in Fig. 1). **a**. A One-Step specimen after 3 months of GTR showing a highly remineralized hybrid layer surface (R), a large remineralized water tree (arrow) that was filled with apatite platelets and a region further away that contained innumerous apatite clusters (asterisk). **b**. At a high magnification, each of the apatite cluster depicted in Fig. 5A consisted of apatite platelets that were arranged into bundles. **c**. A One-Step specimen after 2 months of GTR. A zone of crystallites (asterisk) could be seen in the adhesive layer beneath the resin composite. **d**. Another One-Step specimen after 4 months of GTR with a denser layer of crystallite deposits (asterisk) at almost the same site as the specimen in the previous figure. **e**. A Single-Bond Plus specimen after 2 months of GTR with partial remineralization along the base of the hybrid layer (pointer). Water trees on top of the hybrid layer were filled with electron-dense minerals (open arrowheads). P: polyalkenoic acid copolymer. **f**. These mineral-containing water trees (pointer) extended through the entire adhesive layer. P: polyalkenoic acid copolymer.

Fig.6 FE-SEM micrographs of cryofractured resin-dentin interfaces. Although the results of Single Bond Plus are shown here, the results are generic for both adhesives. **a**. Control specimen retrieved after 4 months. A zone of denuded collagen fibrils (asterisk) could be seen at the base of the hybrid layer (H) that was incompletely infiltrated by resin (pointer). D: mineralized dentin. **b**. Higher magnification view of Fig. 6a showing that the demineralized collagen fibrils appeared smooth and shrunken after dehydration (pointer). **c**. A specimen that had undergone Guided Tissue Remineralization for 2 months. While most of the denuded collagen fibrils were smooth (open arrowhead), a small number of fibrils exhibited a "corn-on-the cob" appearance (pointer). **d**. A specimen that had undergone Guided Tissue Remineralization for 4 months. Most of the denuded collagen fibrils had either a "corn-on-the-cob" appearance or appeared vaguely banded.

Fig.7 A series of schematics illustrating Guide Tissue Remineralization of incompletely resin-infiltrated, acid-etched dentin. **a**. Penetration of polyacrylic acid-stabilized amorphous calcium phosphate precursors into hybrid layers via the resin-sparse, collagen rich regions as well as potentially porous regions within the adhesive layer. **b**. Stage I of Guided Tissue Remineralization (GTR) – coalescence of the fluidic amorphous nanoprecursors within interfibrillar spaces and voids within the adhesive. **c**. Stage II of GTR. Diffusion of polyvinylphosphonic acid molecules into the denuded collagen matrix. These molecules attach to collagen binding sites along the surface of the collagen fibrils. Auto-transformation of the amorphous calcium phosphate nanoprecursors results in the deposition of apatite crystallites along the interfibrillar spaces. **d**. Stage III of GTR. As more polyvinylphosphonic acid molecules diffuse into the collagen fibrils and bind to specific sites along the tropocollagen molecules, intrafibrillar remineralization occurs within the gap zones of the collagen fibrils.

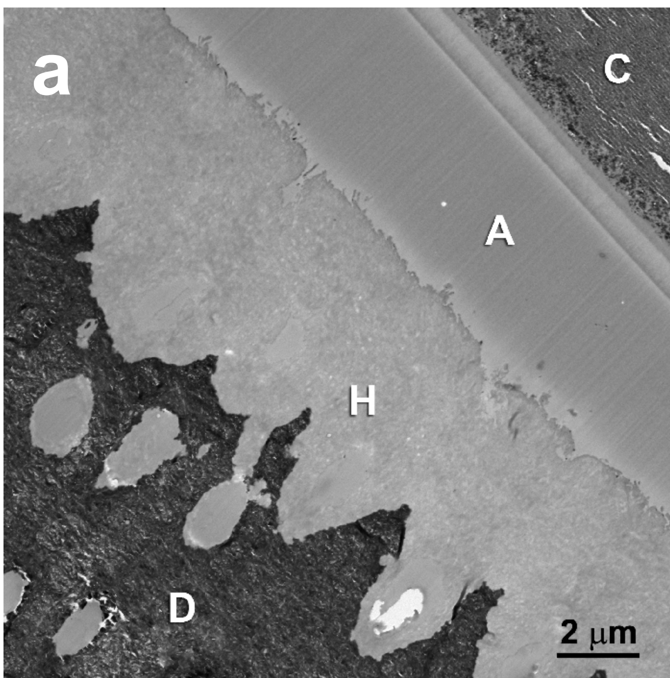
a
C
A
H
D
2 μm

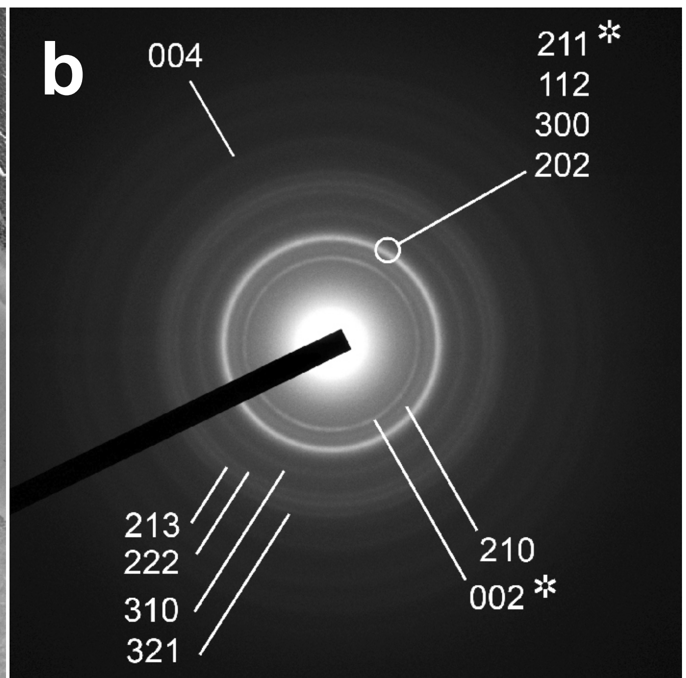
b
004
211 *
112
300
202
213
222
310
321
210
002 *

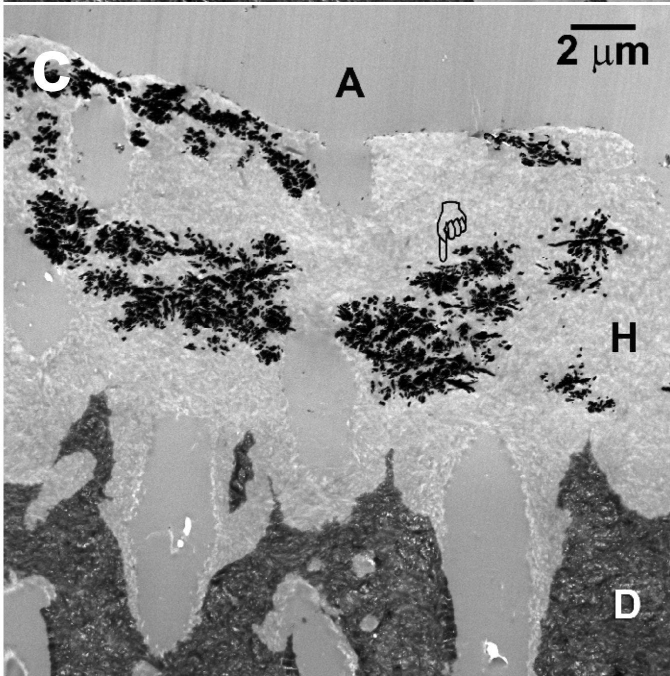
c
2 μm
A
H
D

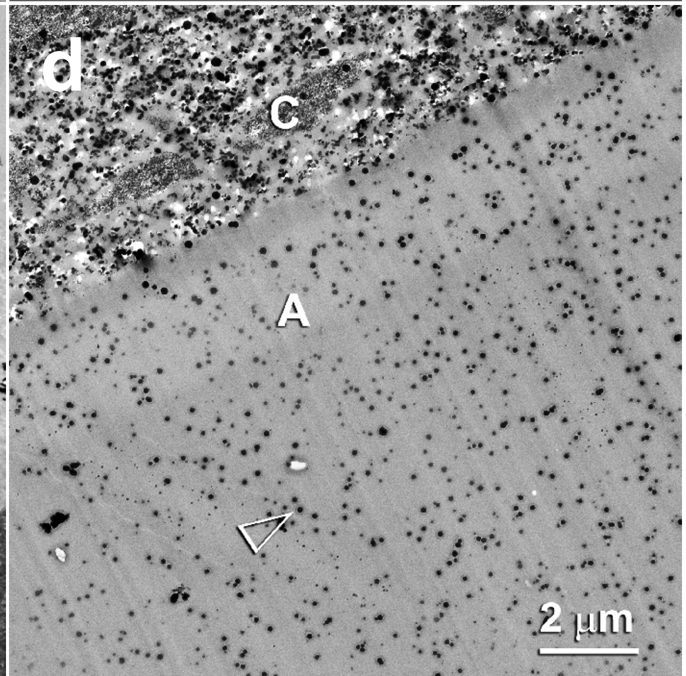
d
C
A
2 μm

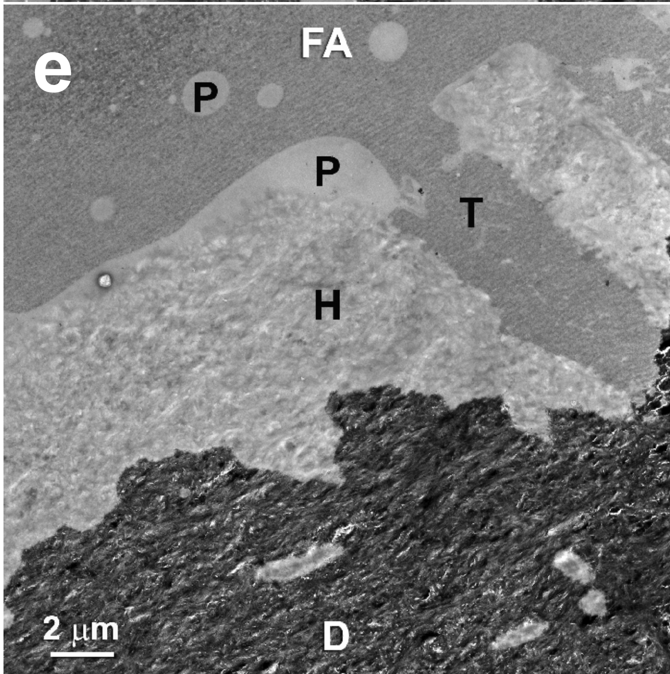
e
FA
P
P
T
H
D
2 μm

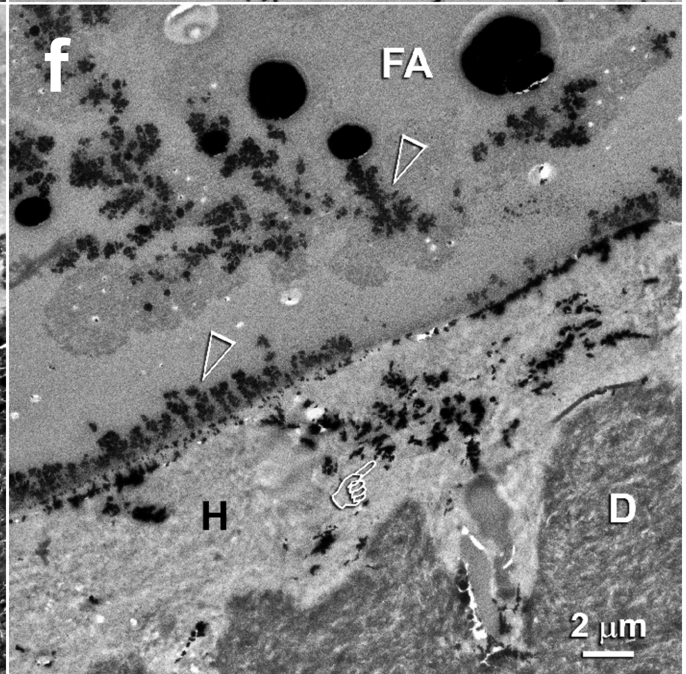
f
FA
H
D
2 μm

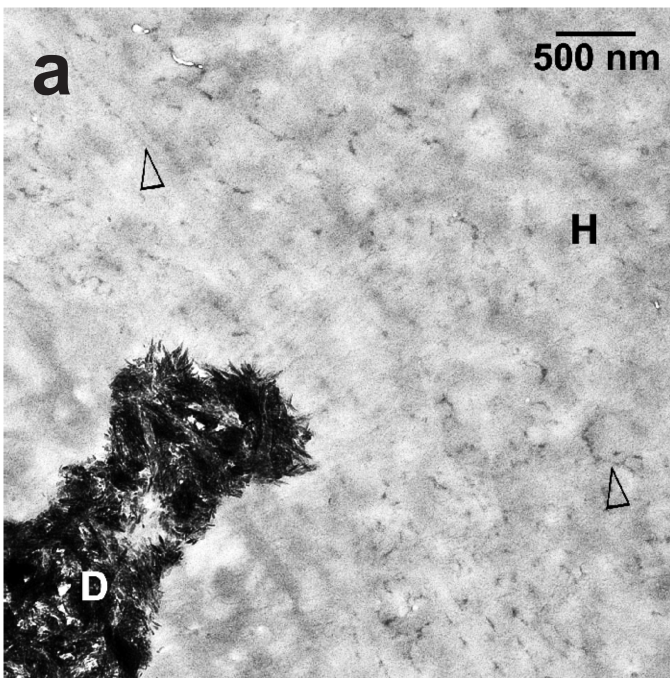

a
500 nm
H
D

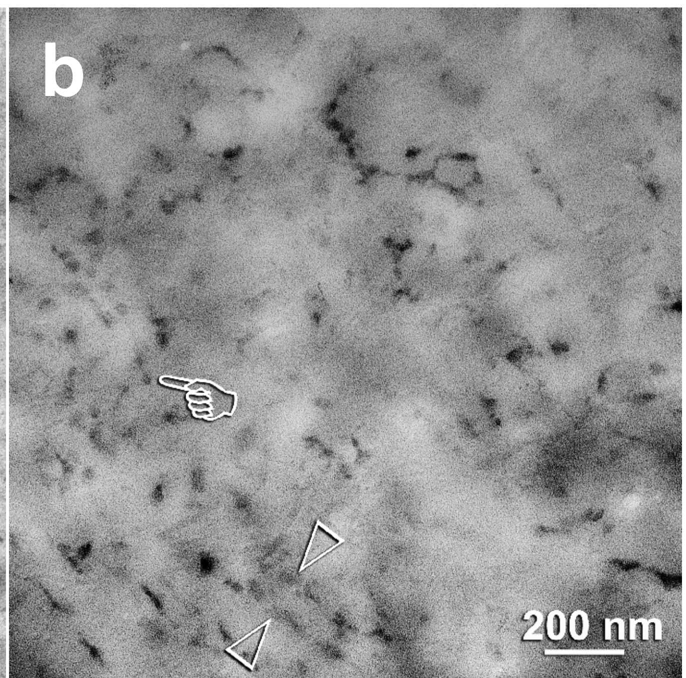

b
200 nm

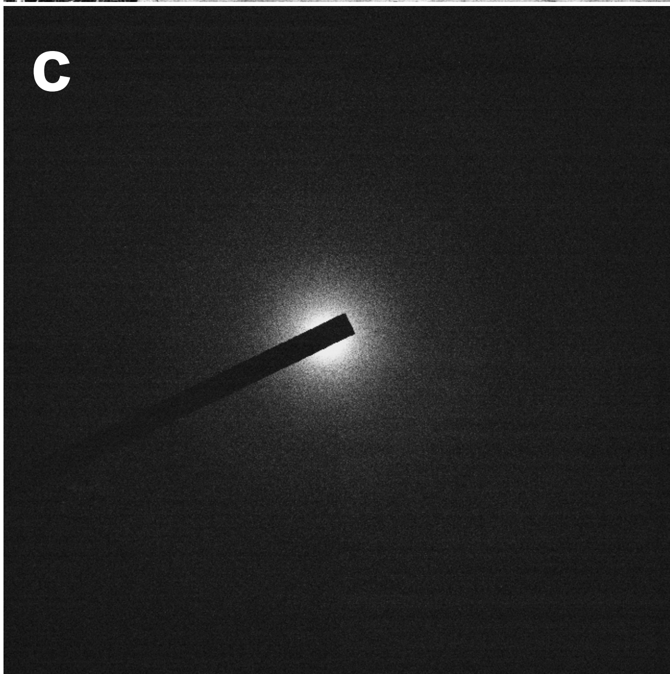

c

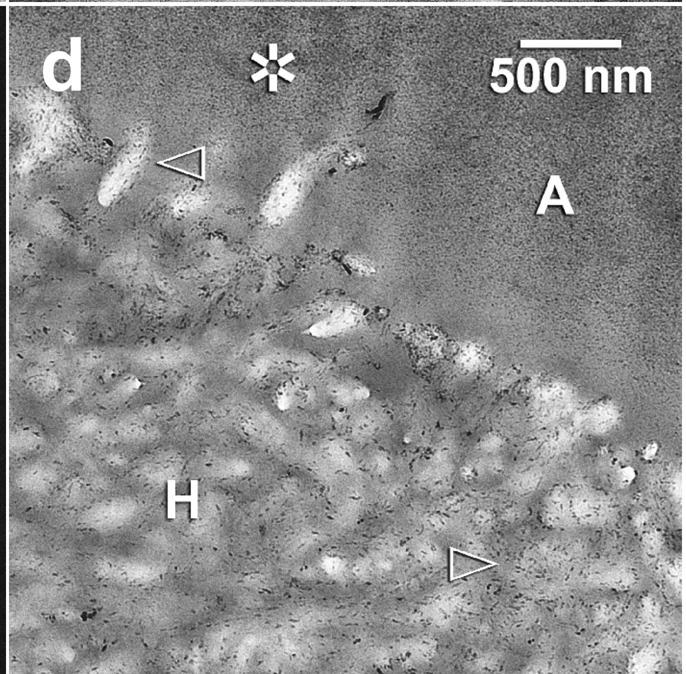

d
500 nm
A
H

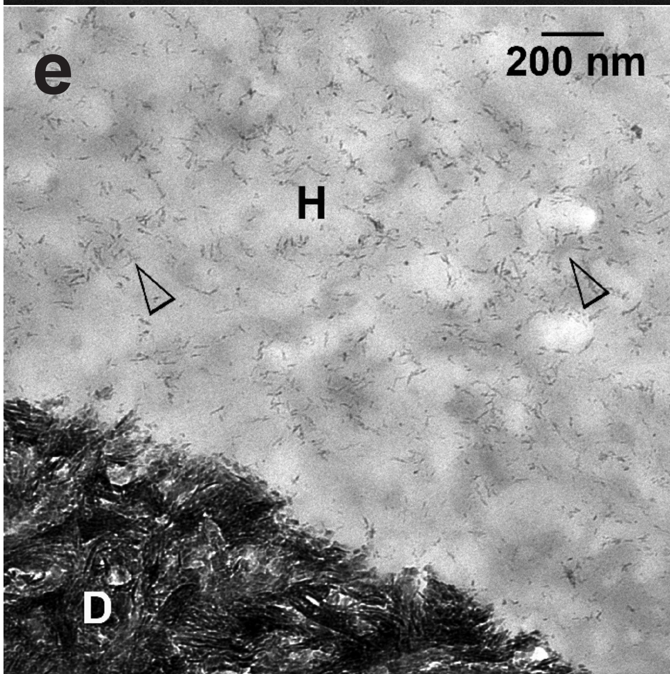

e
200 nm
H
D

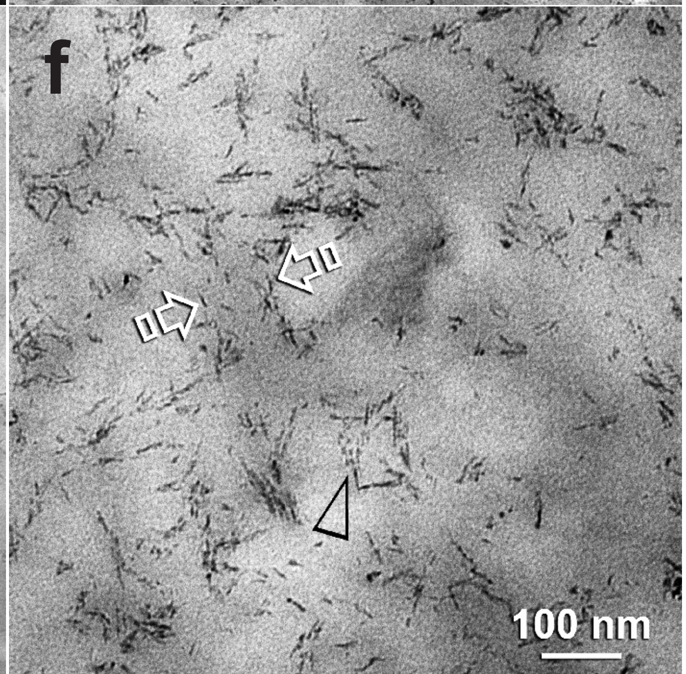

f
100 nm

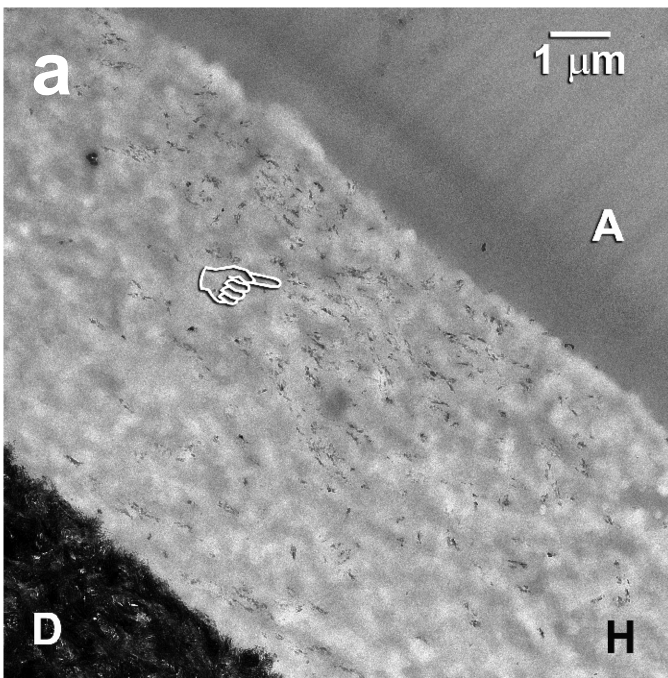
a
1 μm
A
D
H
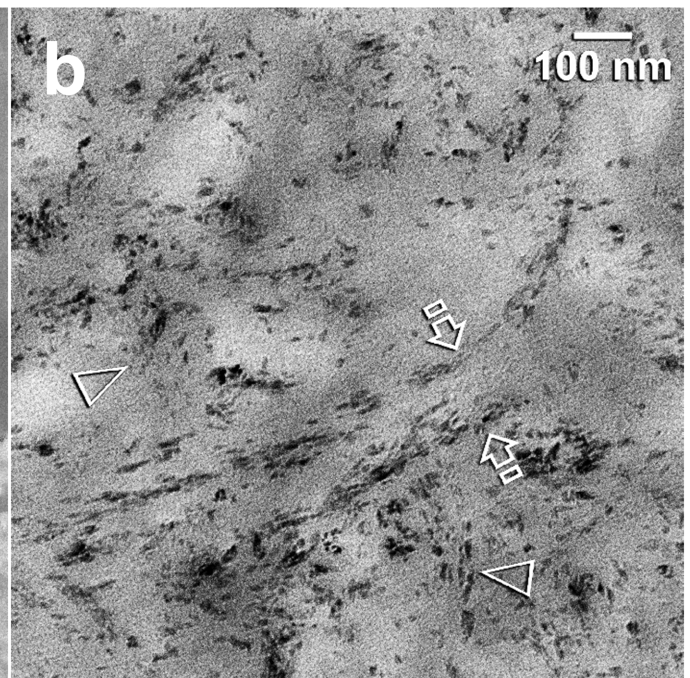
b
100 nm
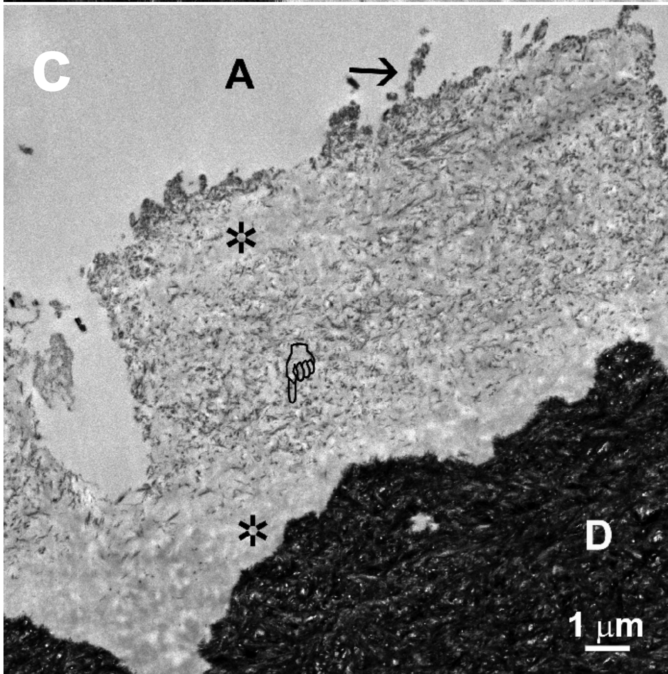
c
A
D
1 μm
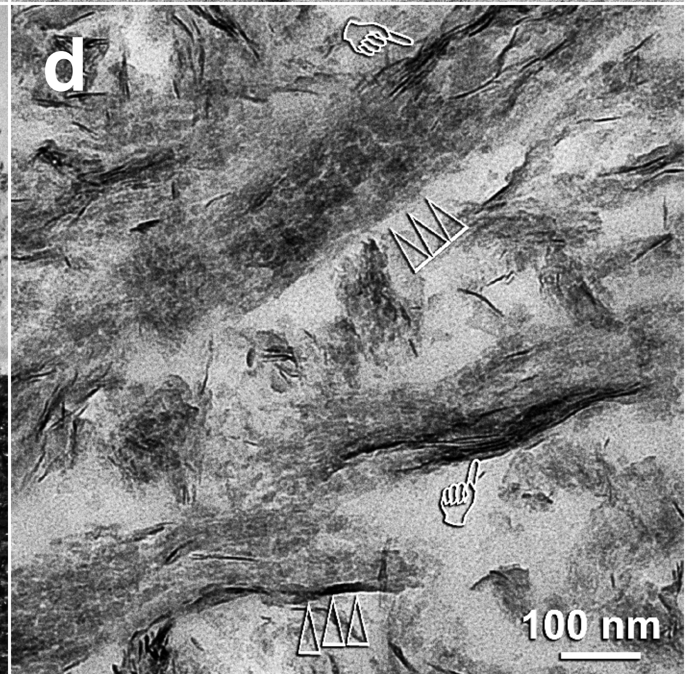
d
100 nm
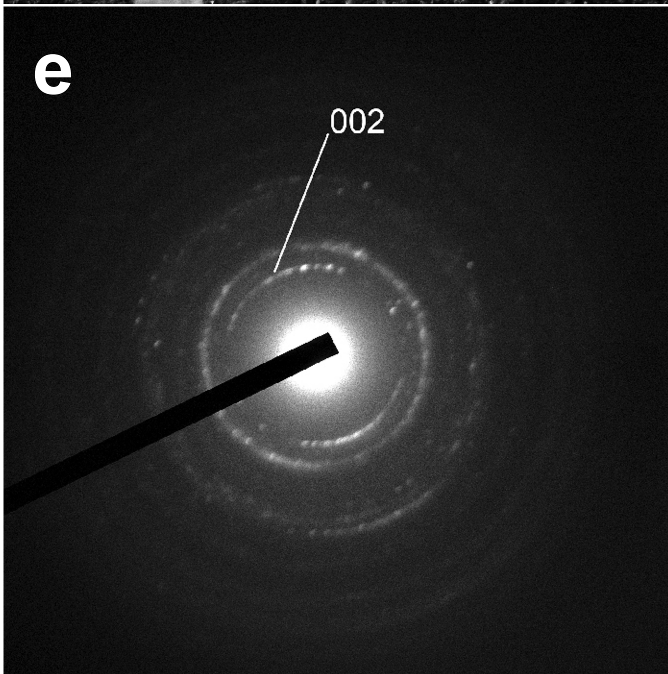
e
002
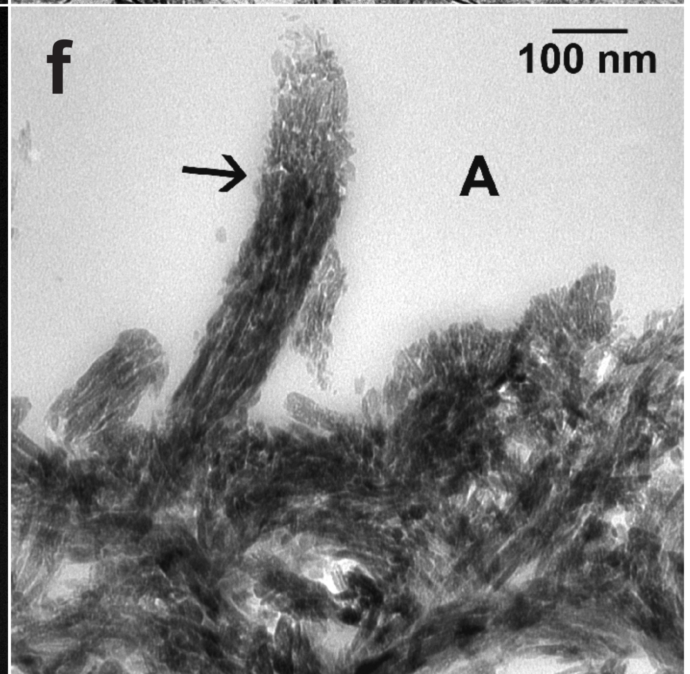
f
100 nm
A

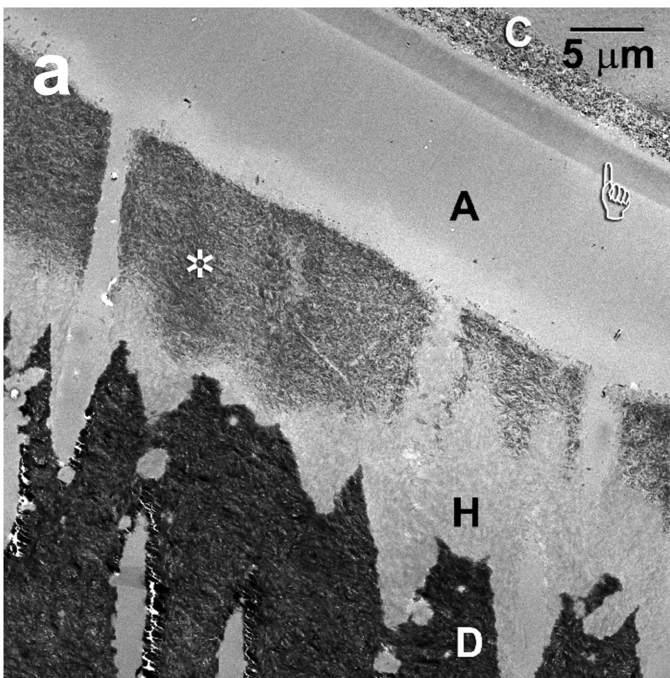
a
c
5 μm
A
*
H
D
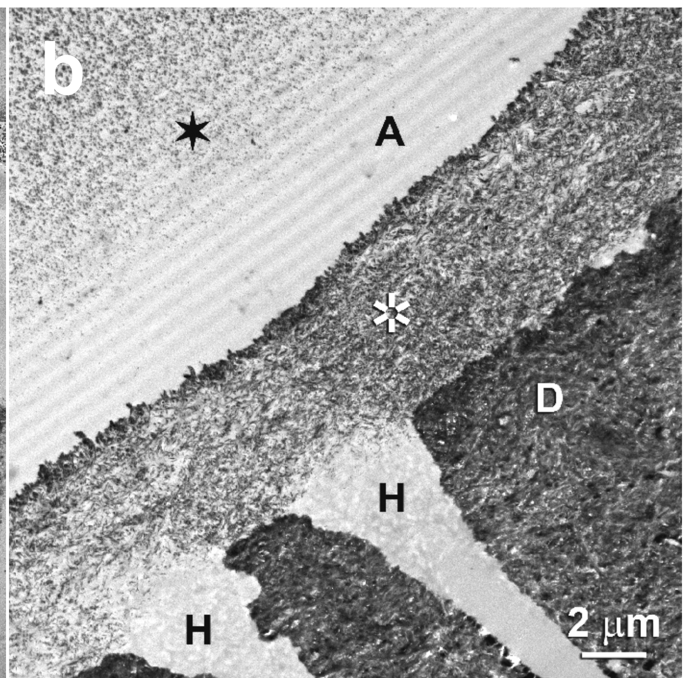
b
A
*
D
H
H
2 μm
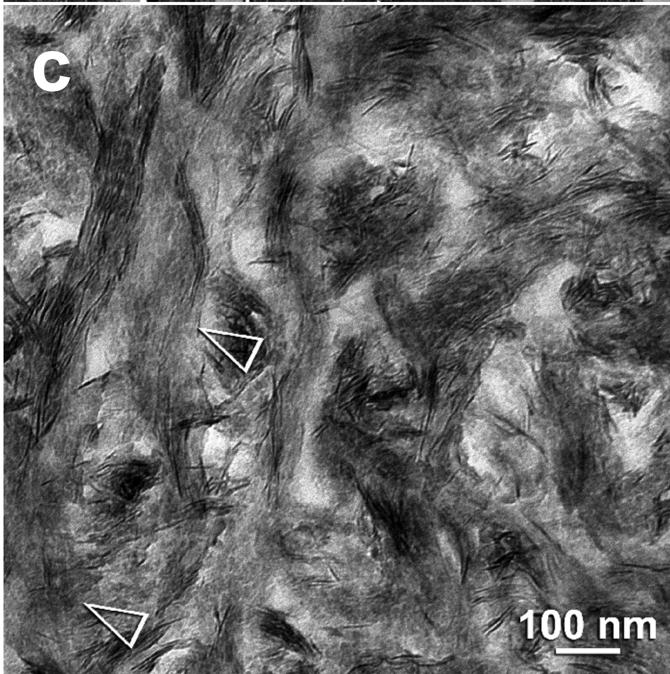
c
100 nm
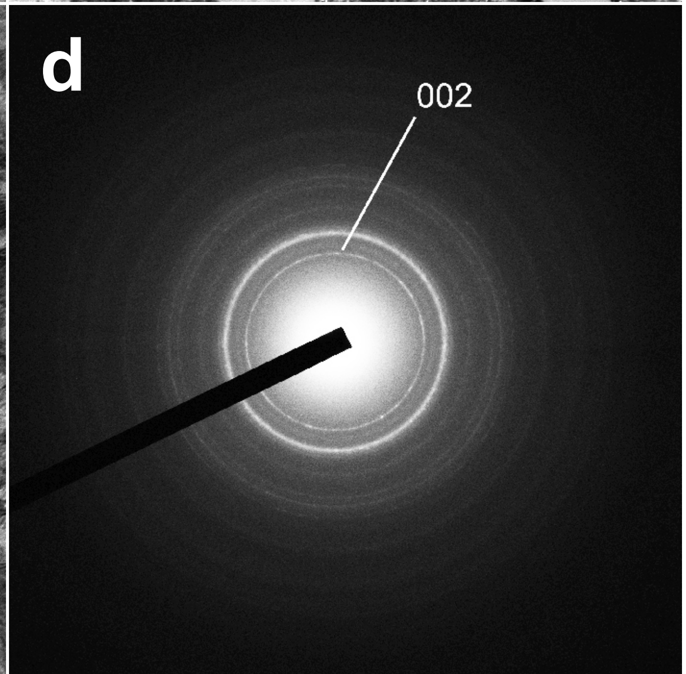
d
002
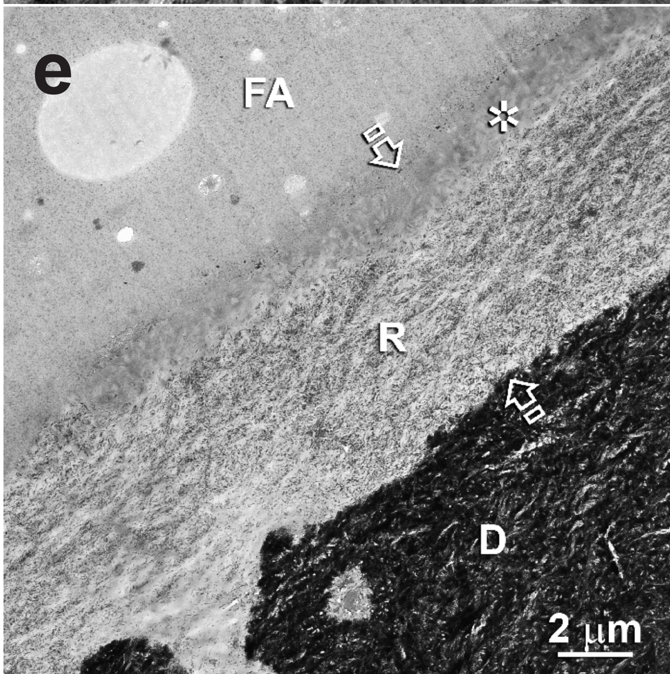
e
FA
*
R
D
2 μm
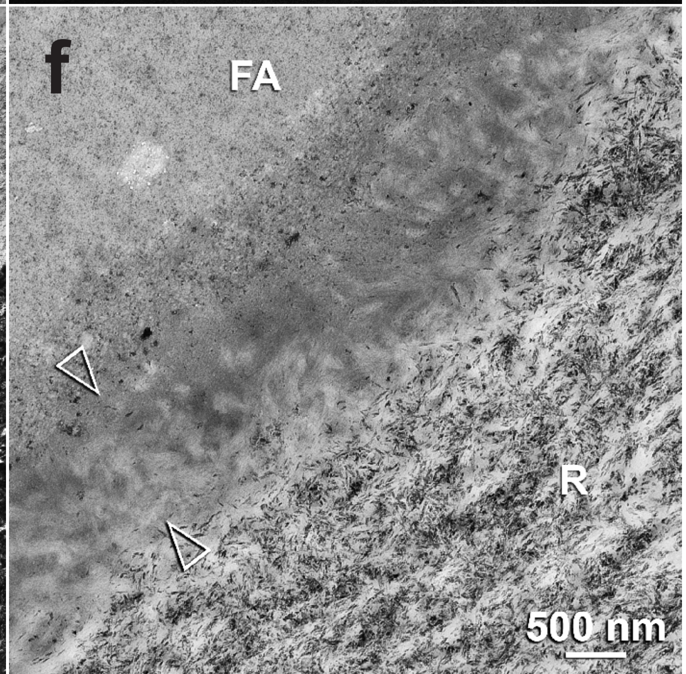
f
FA
R
500 nm

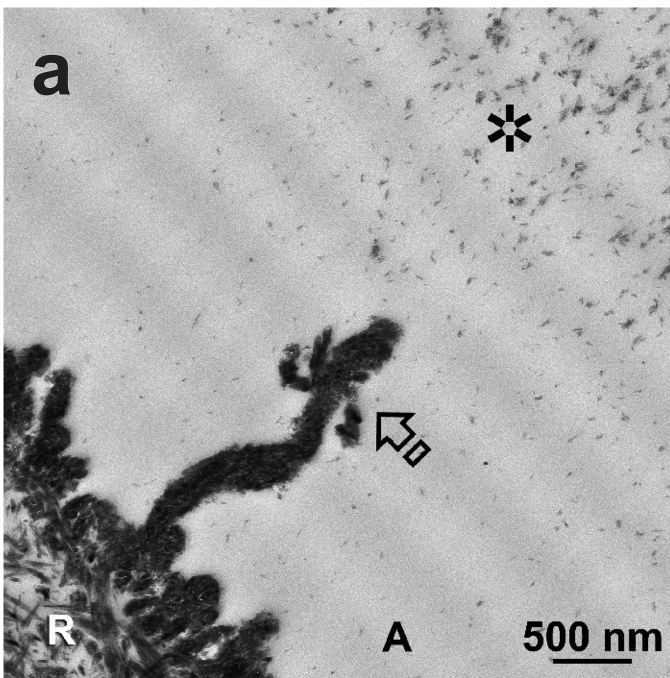
a
R
A
500 nm
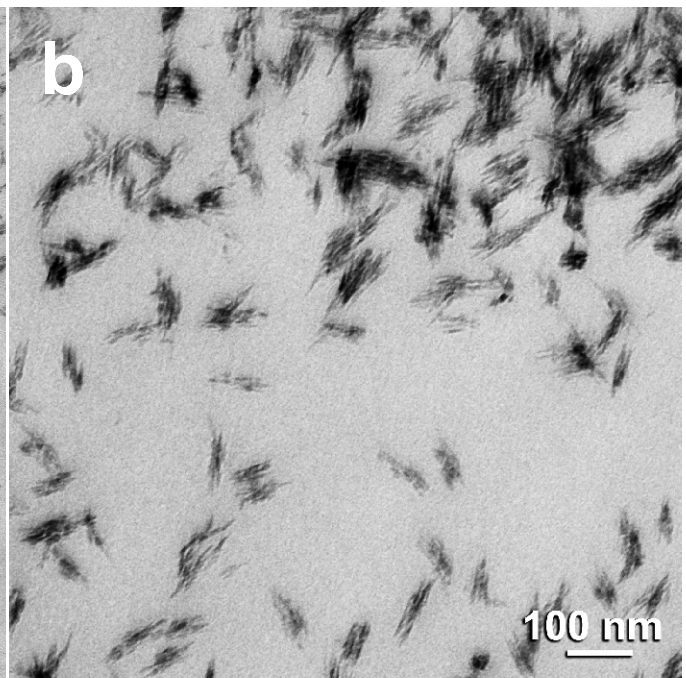
b
100 nm
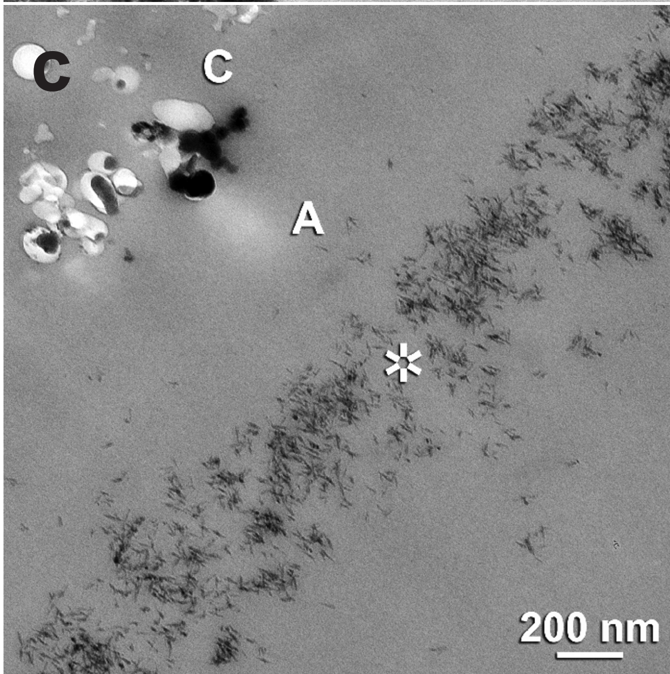
c
C
A
200 nm
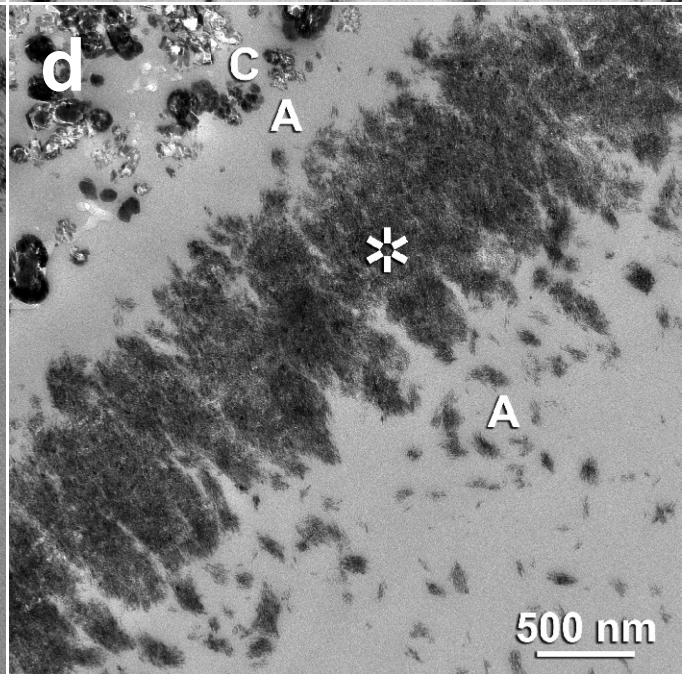
d
C
A
A
500 nm
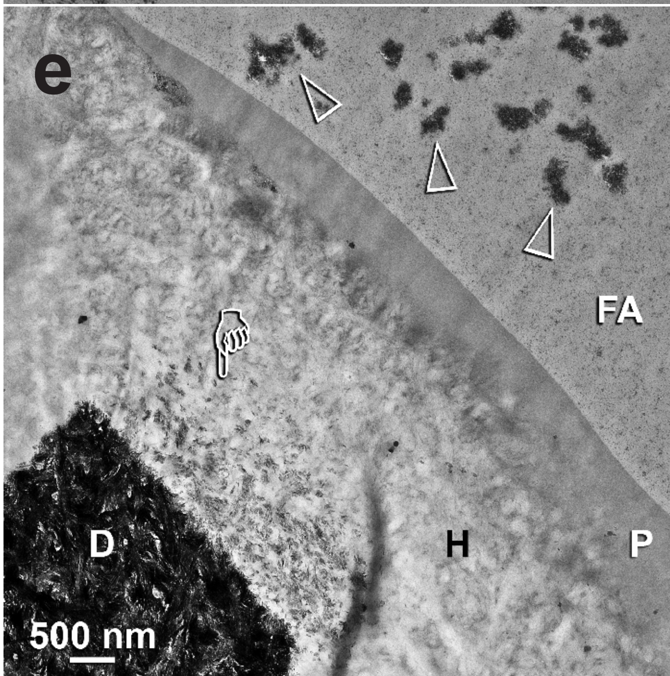
e
FA
D
H
P
500 nm
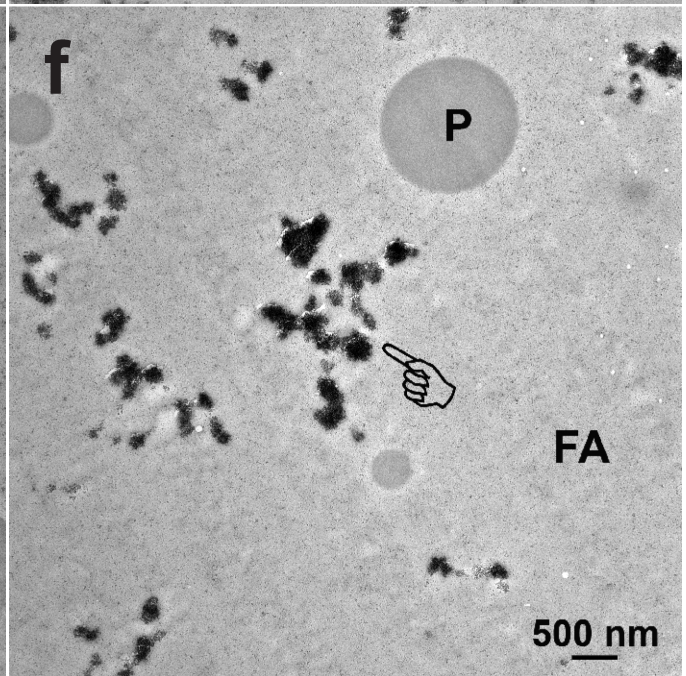
f
P
FA
500 nm

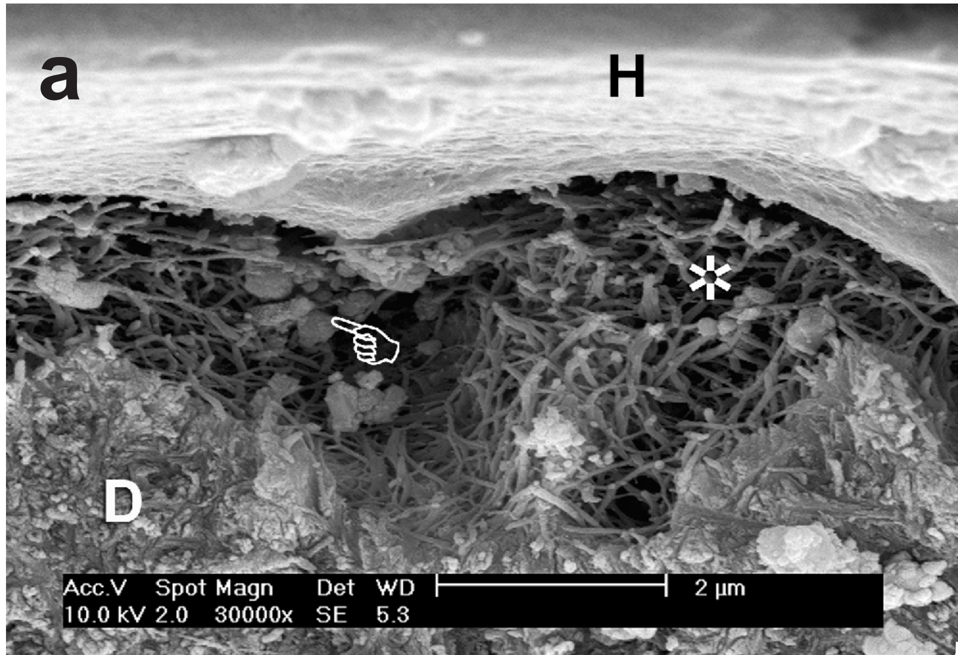
a
H
D
Acc.V Spot Magn Det WD 2 µm
10.0 kV 2.0 30000x SE 5.3

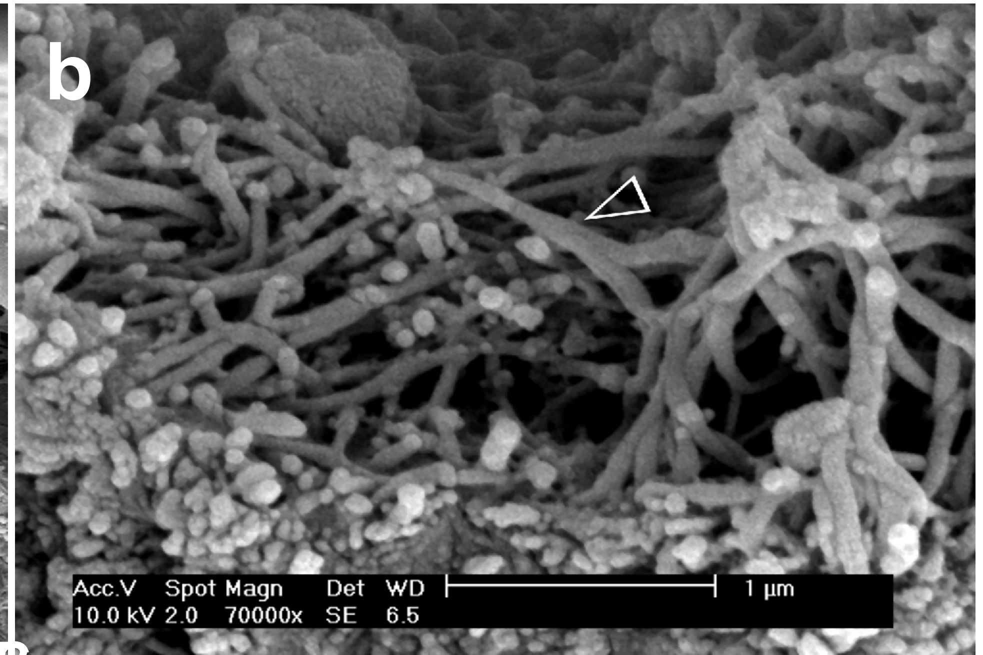
b
Acc.V Spot Magn Det WD 1 µm
10.0 kV 2.0 70000x SE 6.5

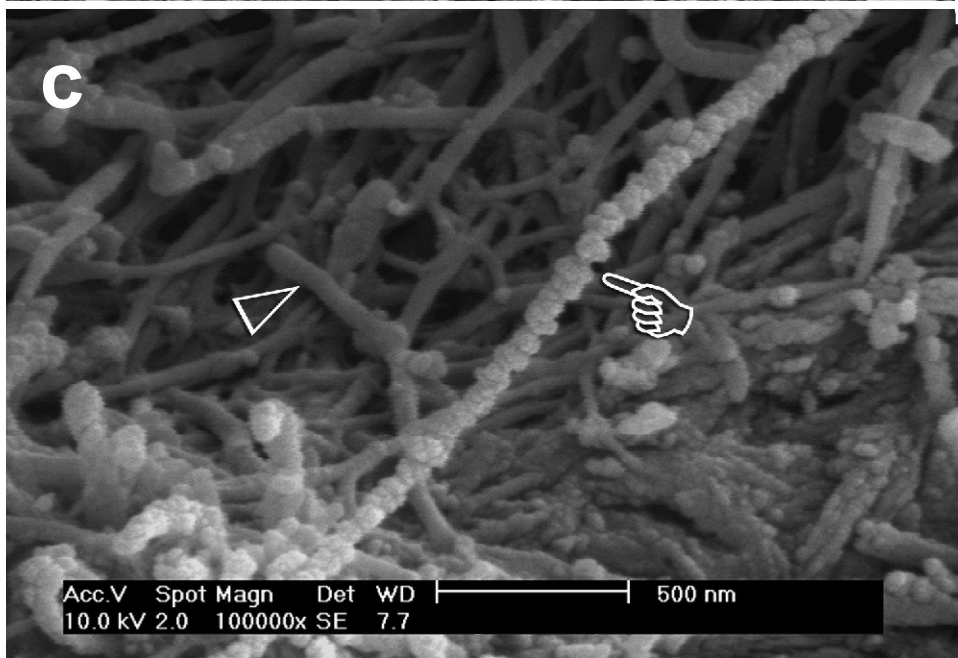
c
Acc.V Spot Magn Det WD 500 nm
10.0 kV 2.0 100000x SE 7.7

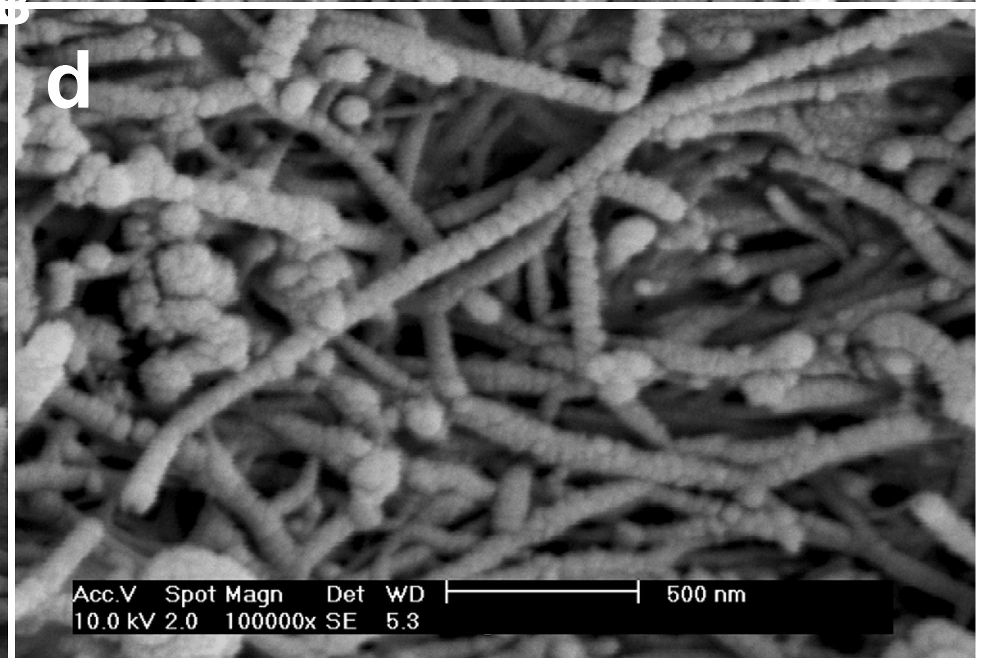
d
Acc.V Spot Magn Det WD 500 nm
10.0 kV 2.0 100000x SE 5.3

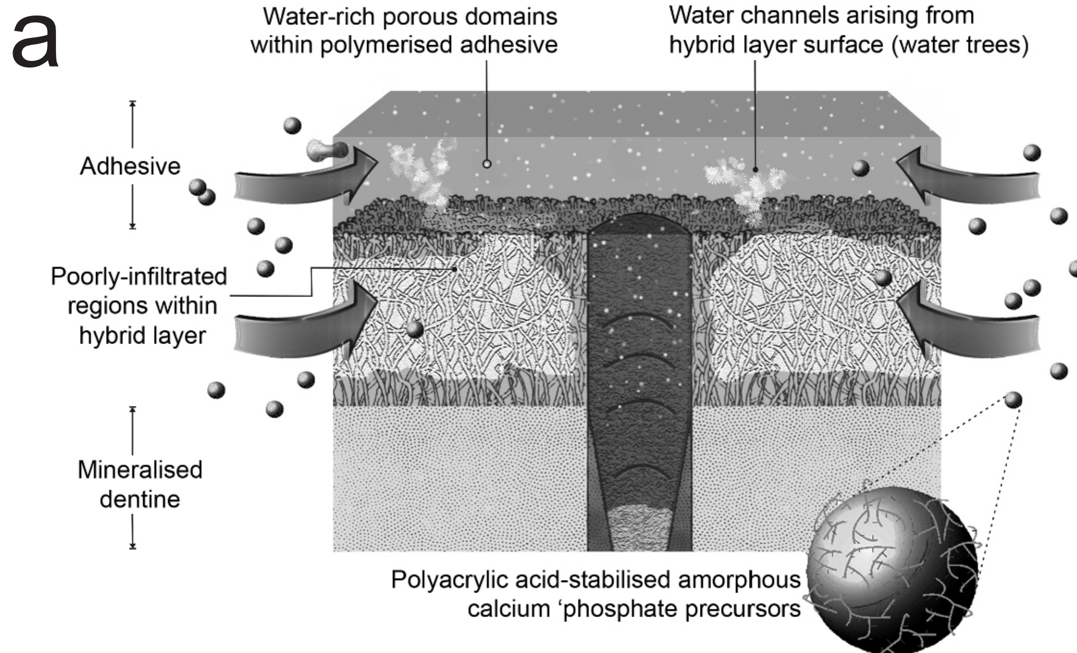
a
Water-rich porous domains within polymerised adhesive
Water channels arising from hybrid layer surface (water trees)
Adhesive
Poorly-infiltrated regions within hybrid layer
Mineralised dentine
Polyacrylic acid-stabilised amorphous calcium ‘phosphate precursors

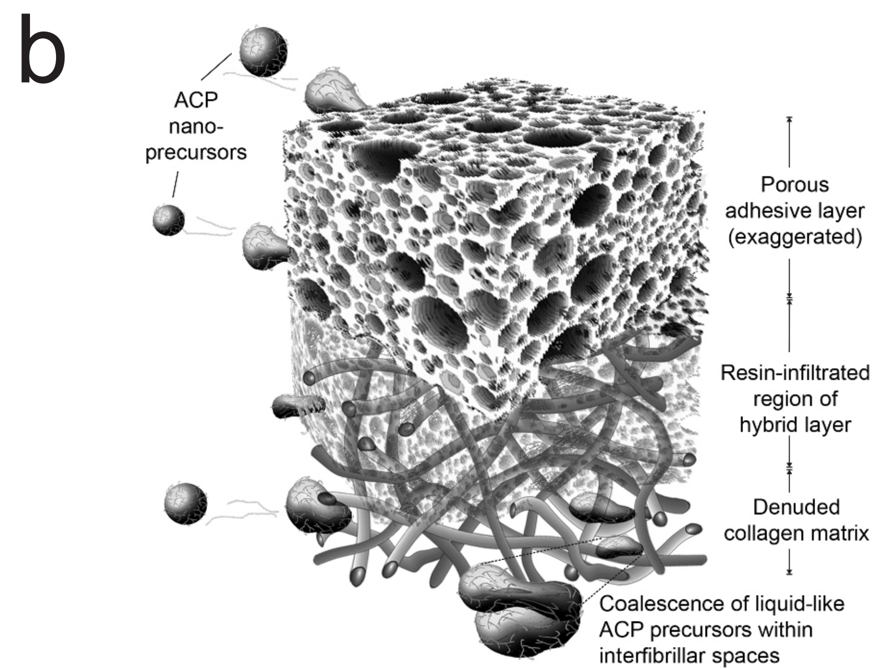
b
ACP nano-precursors
Porous adhesive layer (exaggerated)
Resin-infiltrated region of hybrid layer
Denuded collagen matrix
Coalescence of liquid-like ACP precursors within interfibrillar spaces

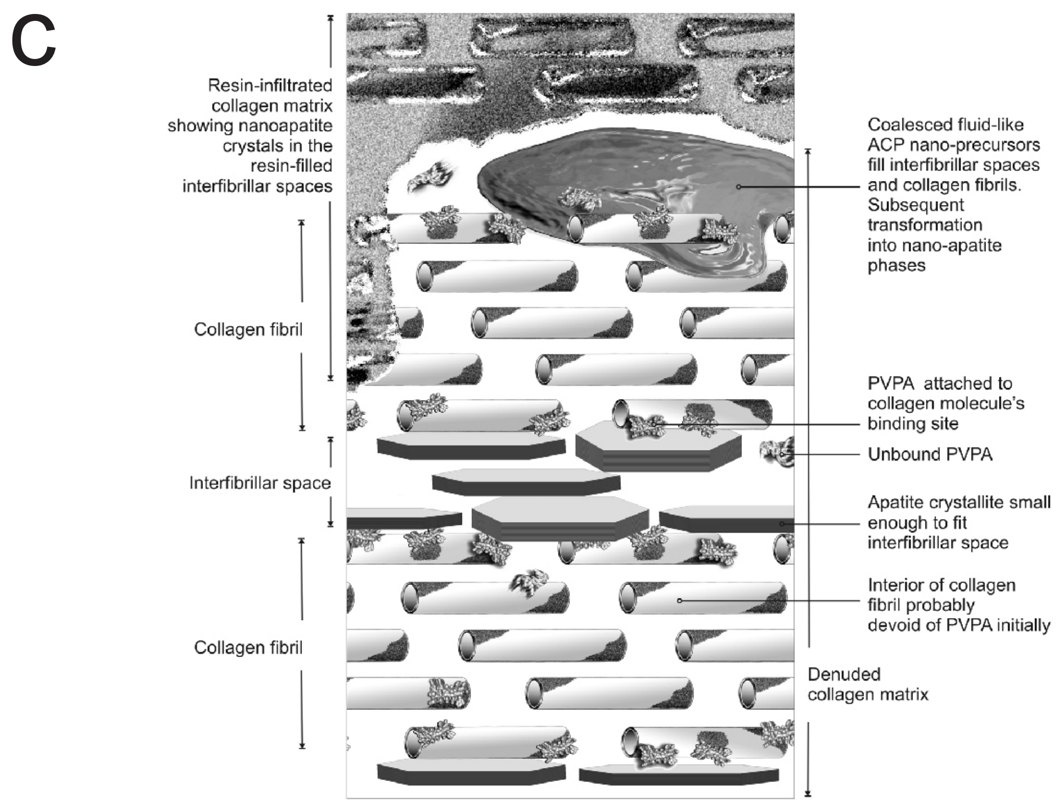
c
Resin-infiltrated collagen matrix showing nanoapatite crystals in the resin-filled interfibrillar spaces
Collagen fibril
Interfibrillar space
Collagen fibril
Coalesced fluid-like ACP nano-precursors fill interfibrillar spaces and collagen fibrils. Subsequent transformation into nano-apatite phases
PVPA attached to collagen molecule's binding site
Unbound PVPA
Apatite crystallite small enough to fit interfibrillar space
Interior of collagen fibril probably devoid of PVPA initially
Denuded collagen matrix

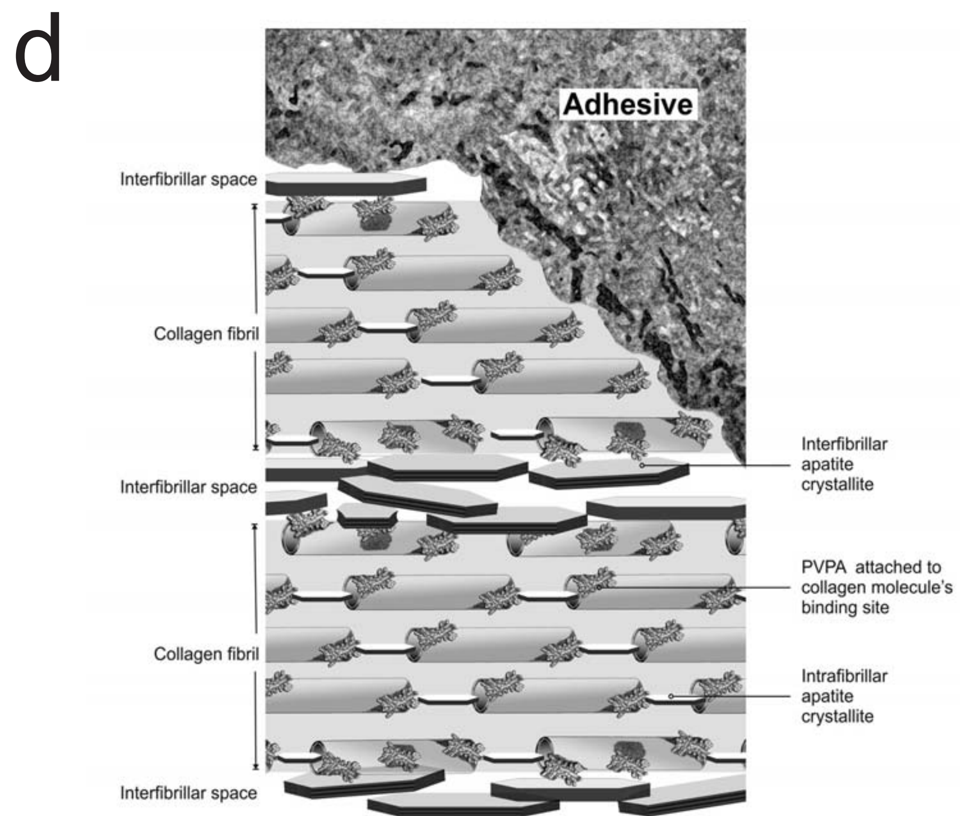
d
Adhesive
Interfibrillar space
Collagen fibril
Interfibrillar space
Collagen fibril
Interfibrillar space
Interfibrillar apatite crystallite
PVPA attached to collagen molecule's binding site
Intrafibrillar apatite crystallite